3

THE LOW-ENERGY PLASMA IN THE JOVIAN MAGNETOSPHERE

J. W. Belcher

The magnetosphere of Jupiter is unique in the solar system because of its large extent and rapid rotation, and because of the prodigious source of plasma provided by the satellite Io. Io and its associated neutral clouds inject $>10^{29}$ amu/s of freshly ionized material into the magnetosphere, producing a plasma torus with a density maximum near the L-shell of Io and a total mass of $\sim 10^{36}$ amu. The innermost region of this torus contains a cool plasma corotating with the planet and dominated by S^+ ions with temperatures of a few eV. At greater distances, beyond 5.6 R_J, the plasma ions are warmer, consisting primarily of sulfur and oxygen ions with temperatures of ~ 40 eV. The plasma electrons here have mean energies of 10 to 40 eV, and exhibit distribution functions which are non-Maxwellian, with both a thermal and suprathermal component. Near Io itself, the Alfvén wave generated by Io gives rise to observed perturbations in the magnetospheric velocities as the ambient plasma flows around the Io flux tube. In the middle magnetosphere, between ~ 8 and ~ 40 R_J, the ions and electrons tend to be concentrated in a plasma disc or sheet that is routinely cooler than its higher latitude surroundings. This plasma tends to move azimuthally but does not rigidly corotate with the planet. The electron density enhancements at the plasma sheet are due primarily to an increase in the electron thermal population with little change in the suprathermal population. At larger radial distances, the suprathermal electrons constitute an increasing fraction of the total electron density and pressure. The mean ion and electron temperature in the plasma sheet increases with increasing distance. Although the mass densities in the middle magnetosphere are dominated by ions with energies of less than 6 keV, the thermal pressure there appears to be due primarily to an energetic ion component with characteristic energies of ~ 25 keV and above. Values of the Alfvénic Mach number range from < 0.1 in the cold inner torus to 2–3 in the plasma sheet.

3.1. Introduction

In 1954, Burke and Franklin [1955] discovered radio emissions from Jupiter at 22.2 MHz. Subsequent observations established the strong control of these decametric emissions by the satellite Io. Thus, a strong satellite–magnetosphere interaction at Jupiter was known well before the start of planetary exploration, and this provided a strong motivation for direct measurements at Jupiter, especially near Io. The first in situ observations of Jupiter were made in December of 1973 with the Pioneer 10 flyby and a year later with the Pioneer 11 flyby. Extensive data were obtained on the magnetic field of Jupiter and on the energy spectrum and spatial distributions of charged particles with energies above ~ 0.5 MeV/nucleon. The Pioneer plasma instrument also provided evidence concerning the plasma environment. Low-energy positive ions (100 to 4800 V), interpreted as protons, were detected in the inner magnetosphere with reported concentrations ranging from 10 to 100/cm^3 and temperatures of the order of 100 eV [Frank et al., 1976]. More recently, Intriligator and Miller [1981] have reexamined the Pioneer data in the Io torus in light of the Voyager results, and report an ion composition and topology similar to that seen by Voyager, as we discuss in the subsection entitled "Comparison with the Pioneer 10 plasma observations." Apparently, the low-energy electron measurements by the Pioneer plasma instruments were seriously

compromised by trapped photoelectrons and secondary electrons [Grard, DeForest, and Whipple, 1977; Scudder, Sittler, and Bridge, 1981].

Just prior to the Pioneer 10 encounter, Brown [1973] reported ground-based optical observations of neutral sodium associated with Io. This observation was followed by the discovery of a torus of singly ionized sulfur [Kupo, Mekler, and Eviatar, 1976]. The S^+ optical radiation these authors observed came from a region inside the orbit of Io (the inner cold torus) and was interpreted by Brown [1976] as originating in a dense ring of cold plasma in that region ($n_e \simeq 3200$/cm^3 and $T_e \simeq 2$ eV). Although this conclusion provoked some discussion at the time, it was not fully appreciated by the space plasma community. However, it clearly marks the discovery of the cold plasma torus at Io. Optical observations of the torus and associated physical processes are discussed at length in Chapter 6.

The Voyager encounters with Jupiter in 1979 have resulted in a dramatic increase in our detailed knowledge of the plasma properties of the magnetosphere. The warm plasma torus was discovered from remote observations of strong emissions from S^{2+}, S^{3+}, and O^{2+} by the Voyager 1 ultraviolet spectrometer [Broadfoot et al., 1979; Sandel et al., 1979]. Measurements by the Planetary Radio Astronomy experiment [Warwick et al., 1979a] and the Plasma-Wave Science experiment [Scarf, Gurnett, and Kurth, 1979] allowed the determination of electron densities along the spacecraft trajectory from characteristic frequencies of various plasma wave emissions. The Low-Energy Charged Particle experiment [Krimigis et al., 1979a] measured the characteristics of the energetic ion population to much lower energies ($\gtrsim 25$ keV) than those of the Pioneer experiments. And, finally, details of the distribution functions of electrons between 10 and 5950 V, as well as those of positive ions in the same energy range, were measured by the Plasma Science experiment [Bridge et al., 1979a]. Such experiments provide a wealth of critical information that is not available from inferences based on remote observations alone. In this chapter, we present a primarily phenomenological account of the in situ observations of low-energy plasma in the Jovian magnetosphere, beginning with the Io torus and proceeding outward. We concentrate primarily on results from the Voyager Plasma Science experiment [Bridge et al., 1977]. The physical mechanisms underlying this phenomenology are considered to a limited extent in Section 3.6, and in more detail in Chapters 10, 11, and 12.

3.2. The Io plasma torus

Bagenal and Sullivan [1981] have constructed comprehensive models of the positive-ion morphology of the Io plasma torus, using positive ion and electron measurements from the Plasma Science experiment on Voyager 1. These authors used the observed density and kinetic temperature of each ionic species and the electron temperatures of Scudder and Sittler (private communication, 1980), in conjunction with the theory appropriate for the ambipolar diffusion of plasma in a rotating, tilted dipole with mirror symmetry about the centrifugal equator. The resulting two-dimensional model of the elementary-charge concentration of positive ions in the Io torus is shown in Figure 3.1. The apparent asymmetry about the centrifugal equator is due to the geometry of the tilted dipole. The distribution of plasma along a given magnetic field line is determined by the balance of electrostatic, centrifugal, and thermal pressure gradient forces. It is apparent from this figure that the torus is divided into two parts: a cold inner region inside of 5.6 R_J where the ions are closely confined to the centrifugal equator, with a vertical scale height of only ~ 0.2 R_J; and a warm outer region with a much larger scale height of ~ 1 R_J. This warm/cold dichotomy of the Io plasma torus is most

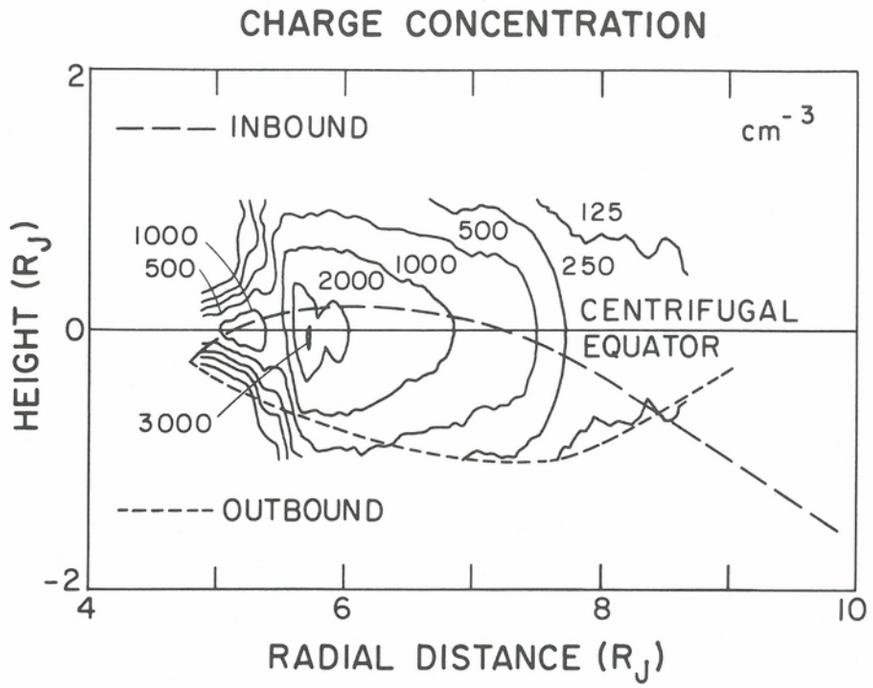

Fig. 3.1. A contour map of elementary-charge concentration in a cylindrical coordinate system based on the centrifugal equator. The map has been constructed from plasma measurements made along the inbound spacecraft trajectory of Voyager 1 by using a theoretical expression for the distribution of plasma along dipolar field lines. Both the inbound and outbound trajectories are indicated by dashed lines. The contours are in units of elementary-charge/cm^3.

dramatically shown in the data presentation of Figure 3.2, which displays the low-energy positive-ion spectra measured along the inbound trajectory of Voyager 1 between 4.9 and 7.0 R_J. To understand this and subsequent figures, we briefly describe the plasma experiment.

The Voyager Plasma Science experiment

The Plasma Science experiment consists of four modulated-grid Faraday cups, three of which (A, B, C) are symmetrically positioned about an axis that generally points toward the Earth, and a fourth (the side sensor, D) oriented at right angles to this direction. Positive-ion measurements are made in all four sensors, and electron measurements in the D sensor alone. The electron measurements are discussed in detail in the subsection entitled "Electron distribution functions in the torus." Throughout most of the inbound leg of the Voyager 1 trajectory (before 0500 UT on March 5, 1979, outside of ~ 10 R_J) the side sensor was pointed in the direction of azimuthal flow of plasma around Jupiter. As the spacecraft approached the planet, the viewing geometry changed rapidly so that after 0500 UT, the look direction of the main sensors was swept into the direction of azimuthal flow and then rapidly away after the closest approach at 1204 UT (Spacecraft Event Time) on March 5, 1979, near 4.9 R_J. Thus, positive-ion data are obtained primarily from Voyager 1 inbound observations; in the

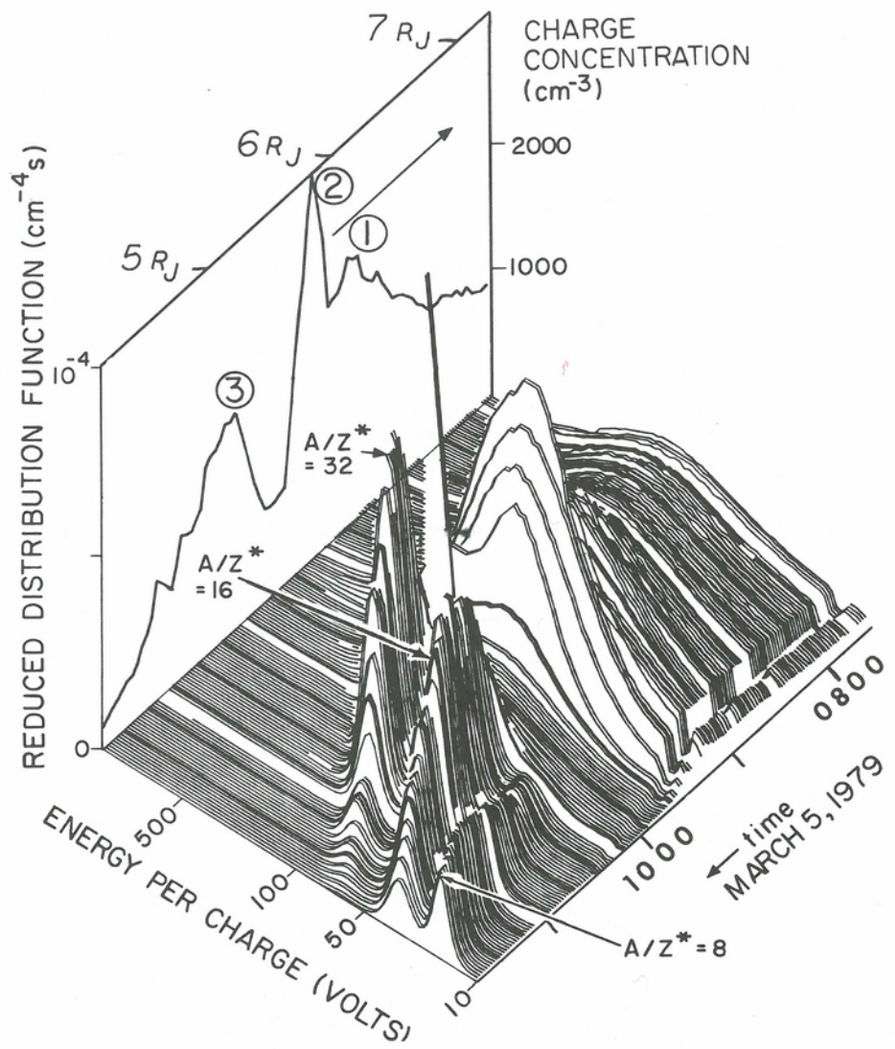

Fig. 3.2. A three-dimensional plot of reduced distribution function against energy per charge for spectral measurements made in the C cup of the main sensor between 0730 UT (7 R_J) and 1145 UT (4.9 R_J) on March 5, 1979. A total of 160 spectra are shown. Two spectra are omitted every 48 min. when the instrument was in a different measurement mode. Every tenth spectrum is emphasized with a darker line. The back panel shows the total positive-ion elementary-charge concentration as a function of time determined from fits to the corresponding spectra. The number features in the back panel are discussed in the text. The notch near 20 V in many of the positive ion spectra is due to interference from another instrument on the spacecraft.

torus proper, the data came from the three Faraday cups in the main cluster, whereas in the middle magnetosphere (outside of 10 R_J), they are obtained primarily from the side sensor. The positive ions are generally transonic to highly supersonic. Because of the unfavorable look directions, positive-ion data outbound are of much poorer quality than inbound, and they will not be discussed here. During the Voyager 2 encounter,

the viewing geometry was similar to that of Voyager 1, but the closest approach distance of 10 R_J precluded observations in the torus.

Each of the four PLS sensors provides an energy-per-charge scan of the positive-ion plasma between 10 and 5950 V. The scan in velocity space is integral in the directions perpendicular to the sensor normal and differential in the direction in velocity space along the sensor normal. Thus, the four energy-per-charge scans provide reduced one-dimensional ion distribution functions for four different directions in velocity space, convolved with the response functions of the sensors (see Appendix A of McNutt, Belcher, and Bridge [1981]). The data in Figure 3.2 are reduced distribution functions from the C sensor of the main cluster, which is essentially aligned with corotational flow during this time interval. The analysis of these spectra is complicated by the presence of many different ionic species in the Jovian magnetosphere. Fortunately, however, for any energy-per-charge instrument, an ion with mass number A and charge number Z^* moving at the same velocity as H^+, appears at an energy-per-charge of A/Z^* times the energy-per-charge of H^+. In the cold region of the torus, after 1016 UT on March 5, the distinct peaks in the energy-per-charge spectra in Figure 3.2 correspond to values of A/Z^* of 8, 16, and 32, assuming a velocity component into the C sensor appropriate for rigid corotation. A different assumption concerning the velocity would, of course, give different values of A/Z^*, but the values of 8, 16, and 32 are plausible (O^{2+}, O^+ or S^{2+}, and S^+). The energy-per-charge of corotating H^+ at this time is below the 10 V threshold of the instrument.

In the cold torus, at least, the interpretation of the positive-ion spectra is thus straightforward: the location of a given ionic peak helps to identify its mass-to-charge ratio as well as providing a quantitative measure of the velocity component into the sensor; the width of the peak provides a measure of the thermal speed for that ionic species and the area under the peak provides a measure of its concentration. In other parts of the magnetosphere, the interpretation is more complex because the peaks overlap (e.g., the warm ion spectra before 1016 UT in Fig. 3.2), but the analysis proceeds in the same spirit – that is, we take advantage of the separation in energy-per-charge of the comoving ionic species due to their different mass-to-charge ratios and their transonic to highly supersonic Mach numbers. In some respects, the electron analysis is less complex because there is only one species of electron and because the electrons are always highly subsonic.

With this brief sketch of the operation of the instrument, we now discuss in turn the observed thermal structure of the torus (ions and electrons), the elementary-charge concentration in the torus, the positive-ion composition in the torus, and finally, plasma velocities in the torus.

Positive-ion temperatures in the torus

In the cold torus, the spectra in Figure 3.2 can be quantitatively analyzed for the density and temperature of each ionic species present, as well as for their common velocity component into the C sensor, by simultaneous fits to a sum of convected Maxwellians. An example of such a fit is given in Figure 3.3. For such cold spectra, the only serious ambiguity in the determination of these plasma parameters arises from the fact that some peaks in A/Z^* do not correspond to a unique ionic species. The most troublesome example in the Io torus and throughout the magnetosphere is the peak at A/Z^* values of 16, the common ratio for O^+ and S^{2+}. Composition and temperature estimates for these two ions are dependent on what fit assumptions are made (e.g., the various ions can be assumed to have either equal temperatures or equal thermal speeds).

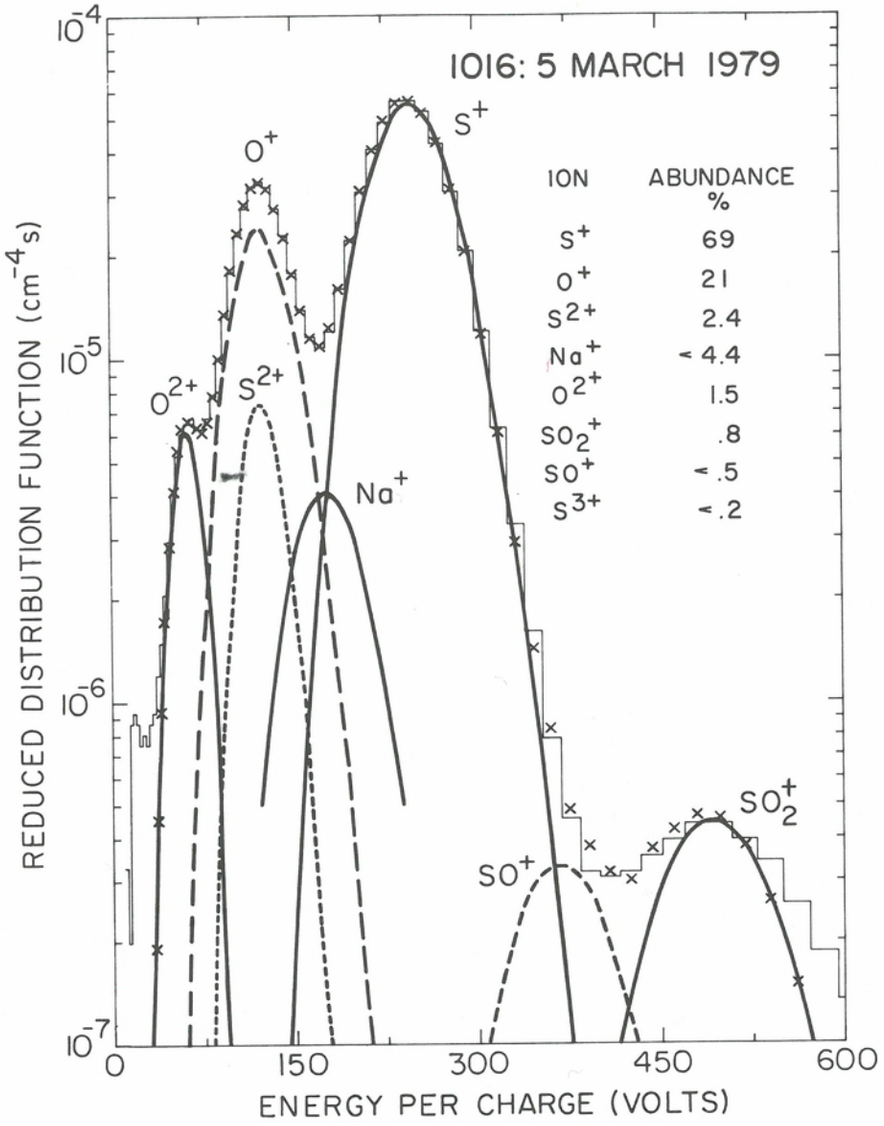

Fig. 3.3. The energy-per-charge spectrum made in the C cup of the main sensor at 1016 UT (5.3 R_J) March 5, 1979. The data are shown as a histogram and the fit to the current in each measurement channel is shown by ×'s. The individual Maxwellian distributions of each ion that make up the reduced distribution function of the fit are shown by the curved lines.

In the warm torus, the ambiguities in the determination of the fit of plasma parameters for each ionic species are more severe than in the cold torus and are more strongly dependent on a variety of assumptions. Whereas, in the cold torus, the Mach numbers of the various adjacent peaks are high enough ($\gtrsim 6$) so that each A/Z^* peak is well separated from adjacent peaks, in the warm torus the Mach numbers are lower ($\gtrsim 3$), and the various heavy-ion peaks overlap (see Appendix A of McNutt, Belcher,

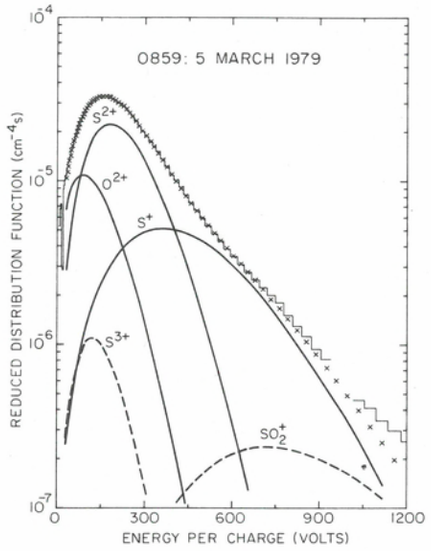

Fig. 3.4. The C cup energy-per-charge spectrum for 0859 UT on March 5, 1979 (6.0 R_J), which has been fit under the assumption that all the ions are corotating with Jupiter and have the same temperature. The data are shown as a histogram and the fit to the current in each measurement channel is shown by ×'s. The individual Maxwellian distributions of each ion that make up the reduced distribution function of the fit are shown by the curved lines.

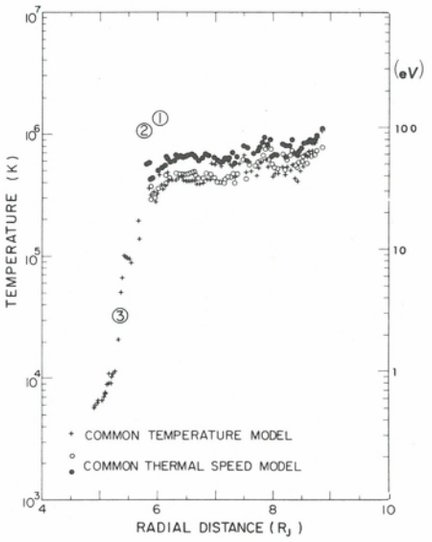

Fig. 3.5. The radial profile of average ion temperature derived from fits to the energy-per-charge spectra of positive ions. The +'s are from the fits where the ions are assumed to have the same temperature. The circles are from the fits where the ions are assumed to have the same thermal speed. With the common thermal speed model the average ion temperature has been calculated assuming the $A/Z^* = 16$ spectral peak to be all S^{2+} (•) or all O^+ (○). The numbered features refer to maxima in the concentration profiles shown in Figures 3.2 and 3.7.

and Bridge [1981]). The plasma parameters obtained depend critically on assumptions concerning composition, temperature, and bulk motion. An example of a fit to a spectrum in the warm torus is shown in Figure 3.4. Bagenal and Sullivan [1981] discuss in detail the results of the fitting procedures in the torus under various assumptions and the subsequent range of plasma parameters that are consistent with the data obtained there.

Figure 3.5 shows the radial temperature profile along the inbound trajectory determined from fits to the ion spectra that are shown in Figure 3.2; uncertainty limits associated with model dependencies are indicated. It is these ion temperatures along the spacecraft trajectory, in conjunction with the electron temperatures discussed in the subsection entitled "Electron distribution functions in the torus," that are used to

construct the model plasma torus in Figure 3.1. The ions beyond about 5.8 R_J have a fairly constant temperature of (6.0 ± 1.5) × 10^5 K (~50 eV), resulting in a vertical scale height of ~1 R_J in that region. This average ion temperature of 50 eV is an order of magnitude less than that expected if the cyclotron speed were equal to the full corotational velocity (see the subsection entitled "Sources of plasma"). As the spacecraft moved inward through the torus, the average temperature decreased sharply inside 5.6 R_J, dropping by a factor of ~50 to less than ~1 eV. This decrease in ion temperature is the cause of the decrease in vertical scale height shown in Figure 3.1.

Electron distribution functions in the torus

In addition to the measurements of positive-ion spectra of Figure 3.2, simultaneous measurements of the electron distribution functions are available. These measurements are made in the D sensor only. As with the ions, the measurements are differential in velocity space for that component of electron velocity along the D cup normal, and integral for velocity components transverse to that normal. Because only one sensor is used, the electron measurements do not contain complete information on the full three-dimensional electron distribution function. However, the electrons are highly subsonic, and with the assumption of isotropy, one can unfold an excellent representation of the electron distribution function. Unfortunately, the low-energy instrumental threshold of 10 V leaves a gap in the energy coverage, and this gap is particularly severe in the cold region of the torus, where the thermal electron temperatures are ~5 eV or less. An equally serious problem in the electron analysis is the effect of spacecraft charging in the high-density regions of the torus. In these regions the spacecraft did apparently achieve a negative potential on the order of a few tens of volts, which has left the final analysis of the electron spectra in the torus (especially the absolute concentrations) incomplete pending a more thorough treatment of the charging problem at high concentrations. In the lower density environment outside of the torus, the charging problem is reasonably well understood and the effects of spacecraft potential can be self-consistently taken into account [Scudder, Sittler, and Bridge, 1981]. In any case, the electron temperature can be determined independently of the concentration, and the temperature profile of the thermal electrons in the torus qualitatively resembles that of the ions. Scudder, Sittler, and Bridge [1981] find three relatively well-defined subregimes of the plasma torus: (a) the cold inner torus, with $T_e \lesssim 5$ eV; (b) the temperate middle torus, with $T_e \simeq$ 10–40 eV; and (c) the hot outer torus just beyond 8 R_J with $T_e \gtrsim 100$ eV. This last regime is the inner edge of the radially extended plasma sheet (see Section 3.4).

For illustration, Figure 3.6 shows electron distribution functions as measured at 5.5, 7.8, and 8.9 R_J. All of these spectra have well developed thermal populations that are well fit by Maxwellian distributions (the "core" electrons, in analogy with solar wind nomenclature). They also exhibit distinct suprathermal tails (the "halo" electrons). In each panel, the subscript "e" refers to the parameters characterizing the electron distribution as a whole, the subscript "C" to parameters characterizing the Maxwellian fit to the thermal population, and the subscript "H" to the parameters of the suprathermal population. The coldest electron spectrum shown ($T_e = 5$ eV), at 5.5 R_J, occurs near the precipitous drop in ion temperature shown in Figure 3.5. In addition to illustrating the cooling of the thermal electron population with decreasing radius, Figure 3.6 also illustrates the increasing importance of the suprathermal electron population with increasing radius. For example, the suprathermal fraction by number varies from 0.02% at 5.5 R_J to 8% at 8.9 R_J. We will find that this trend continues as we move into the middle magnetosphere. The existence of these "hot" and "cold" populations of

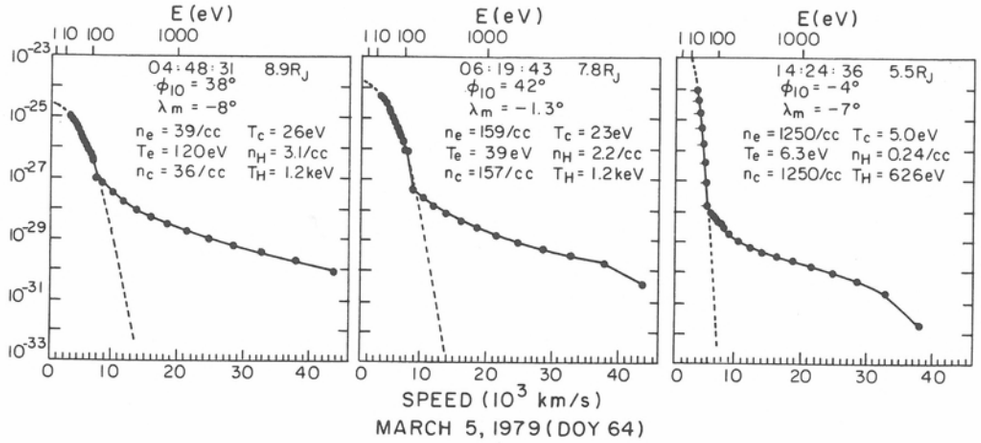

Fig. 3.6. Plots of the electron distribution function measured at three different times in the inner magnetosphere by the Voyager 1 Plasma Science experiment. The measurement times, radial distance of spacecraft from Jupiter, System III longitude of spacecraft relative to Io, and dipole magnetic latitude of the spacecraft are indicated. The connected points are data points, and the dashed lines are Maxwellian fits to the thermal population of electrons.

electrons has also been deduced from the characteristics of various plasma wave emissions. In particular, at the time of the center distribution function shown in Figure 3.6, Coroniti et al. [1980] concluded that the observations of plasma chorus by the Plasma Wave Science experiment required the presence of suprathermal electrons with a characteristic energy of 1 keV and a fractional density of 1.1%, in good agreement with the population actually measured. In addition, Birmingham et al. [1981] using the characteristics of emissions observed by the Planetary Radio Astronomy experiment, have inferred the existence of a hot electron population. These authors also predicted a variation of T_c/T_H that decreases as the spacecraft moves from the hot outer torus to the cool inner torus, a prediction qualitatively in agreement with the distributions of Figure 3.6. Finally, an analysis of the thermal emissions from the torus also calls for the presence of such electrons (see Chap. 12).

Elementary-charge concentrations in the torus

Even though we cannot at present derive absolute electron concentrations from the Plasma Science electron measurements in the high density torus, we can derive an estimate of that concentration from the positive-ion measurements (which are less affected by spacecraft charging) and the requirement of charge neutrality. Figure 3.7 show the elementary-charge concentration along the inbound trajectory for ions with values of $A/Z^* \geq 8$, as determined from fits to the ion spectra shown in Figure 3.2. The three local maxima labeled in Figure 3.7 are the same as those labeled in the back panel of Figure 3.2. We also show in Figure 3.7 the determinations of the total electron concentration by the Planetary Radio Astronomy experiment, which should match the elementary-charge concentration from the positive-ion fits, if contributions from ions with $A/Z^* < 8$ are small. Because the agreement between these two determinations is good, we conclude that lighter ions do not contribute a significant amount of charge concentration at these latitudes and distances. For an estimate of their contribution at higher latitudes at these distances, see Tokar et al. [1982].

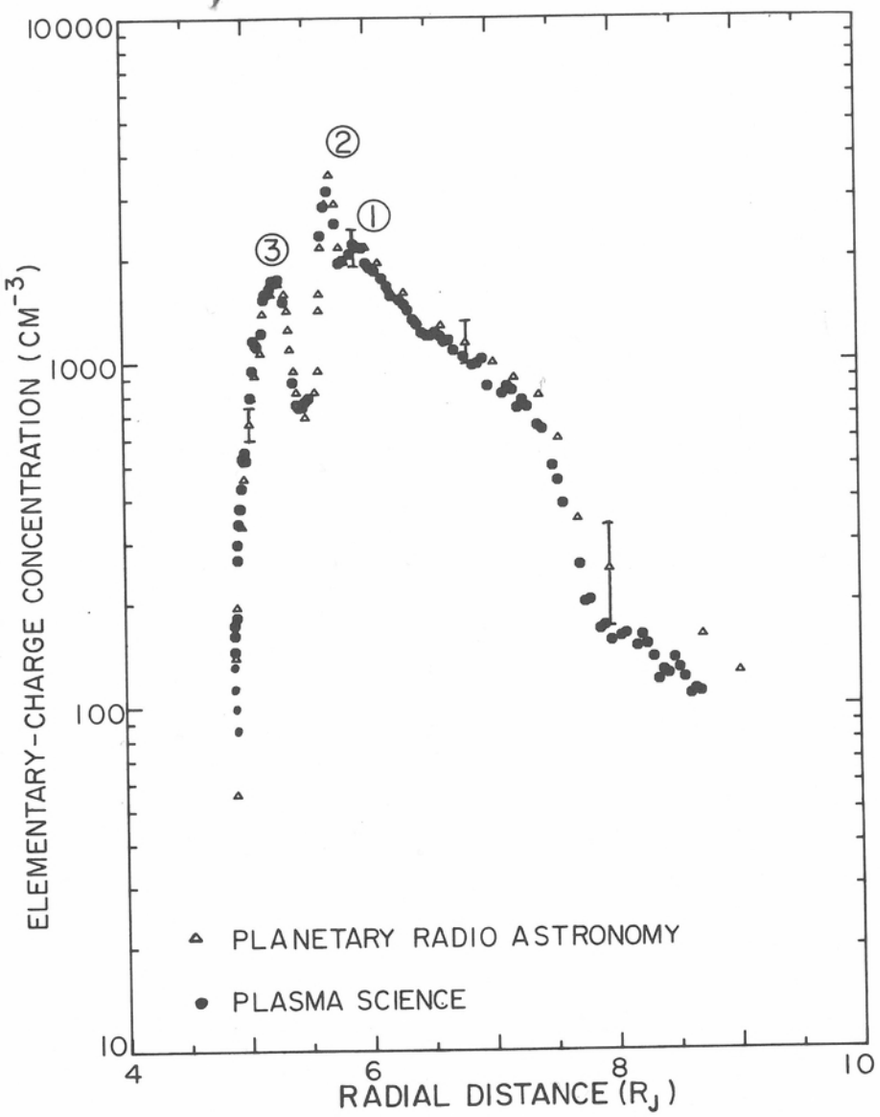

Fig. 3.7. The radial profile of charge concentration along the inbound trajectory of Voyager 1. The Plasma Science measurements (•) are of the elementary-charge concentration of positive ions derived from fits to positive-ion energy-per-charge spectra. The Planetary Radio Astronomy data (Δ) from Birmingham et al. [1981] are electron concentrations determined from the cutoff frequency of plasma wave modes (the uncertainties in the Planetary Radio Astronomy determinations are shown by vertical bars). The numbered features are described in the text, and are also indicated in Figures 3.2 and 3.5.

The detailed features of the inbound elementary-charge concentration shown in Figure 3.7 are best understood in close comparison with the inbound temperature profile of Figure 3.5 and the two-dimensional contour model of Figure 3.1. The outer edge of the torus is indicated by the rapid increase in concentration in Figure 3.7 as the spacecraft moved inside of $\sim 7.5\ R_J$. After crossing the centrifugal equator at 7.1 R_J

(see Fig. 3.1), the spacecraft remained less than 0.15 R_J above that equator and traversed the core of the warm torus. The in situ concentration built up to a broad local maximum around the orbit of Io at 5.95 R_J (Peak 1 in Fig. 3.7). The spacecraft then passed over the small region of peak concentrations in the contours shown in Figure 3.1, giving rise to the sharp spike (Peak 2) in the in situ concentration profile of Figure 3.7 ($\sim$ 3100/cm^3 at $\sim$5.7 R_J). The Planetary Radio Astronomy experiment recorded a peak concentration of 3500/cm^3 around this time. However, there were few measurements of such large values and these were all measured near 5.75 R_J. Radially inward of 5.7 R_J, the elementary-charge concentration dropped rapidly by a factor of $\sim$5 to a local minimum of 740/cm^3 at $\sim$5.4 R_J. The spacecraft then crossed the centrifugal equator again, near the crest of the inner localized knoll in the concentration contours of Figure 3.1. This inner knoll is caused by the collapse of the torus plasma toward the centrifugal equator as it diffuses inward and cools (see Fig. 3.5 and the subsection entitled "Diffusive transport"). The crossing of this knoll resulted in a third local maximum in elementary-charge concentration of 1740/cm^3 at $\sim$5.2 R_J (Peak 3 of Fig. 3.7) before a final rapid decrease as the spacecraft made its closest approach to Jupiter at 4.89 R_J.

Bagenal and Sullivan [1981] found that the global structure on the outbound pass was nearly indistinguishable from that on the inbound pass, with similar features at similar L-shells, when the offset of the tilted dipole was taken into account. The main effect of including the offset is to change the apparent outbound trajectory shown in Figure 3.1. When this was done, the electron concentration profile predicted for the outbound structure from inbound data was in good agreement with that measured by Warwick et al. [1979a]. Consequently, the Plasma Science measurements show no clear evidence that the electron concentration varies in either longitude or local time, even though enhanced ultraviolet emission has been reported from the warm torus in the dusk quadrant [Sandel, 1980], and enhanced S^+ emission has been reported from the cold torus in the active sector [Trafton, 1980]. In contrast, radical changes in plasma properties are observed over radial spatial scales as short as $\sim 10^4$ km, for example the temperature gradient at 5.5 R_J ($\sim 7 \times 10^5$ K R_J^{-1}).

Positive-ion composition in the torus

Major ionic species. In addition to these variations in overall concentration in the inner magnetosphere, there is considerable variation in the relative abundances of the different ionic species. Table 3.1 from Bagenal and Sullivan [1981] presents in situ concentrations determined from fits to energy-per-charge spectra at 4.96 and 5.3 R_J (in the inner cold torus); at 6.0 R_J (in the outer warm torus); at 8.6 R_J (just outside the torus); and at four of the many locations in the plasma sheet of the middle magnetosphere where there are well-resolved spectral peaks (11.8, 20, 28, and 42 R_J). The spectra from the middle magnetosphere are included here for completeness in the discussion of composition (the middle magnetosphere is discussed in detail in Sec. 3.4). At 6.0 and 8.6 R_J, where the various peaks are unresolved, the results of fitting the spectra assuming different thermal models are tabulated.

From the warm torus outward into the middle magnetosphere, the composition remains fairly constant. The major ionic species are some combination of O^+ and S^{2+} at an A/Z^* value of 16. Next in importance are O^{2+}, S^{3+}, and S^+, with the relative abundance of S^{3+} and O^{2+} varying considerably depending on assumptions about the thermal state of the plasma. In the cold inner torus the composition is significantly different. The dominant ion is S^+, with O^+ next in importance, and with few ions of higher ionization states (S^{2+}, S^{3+}, O^{2+}).

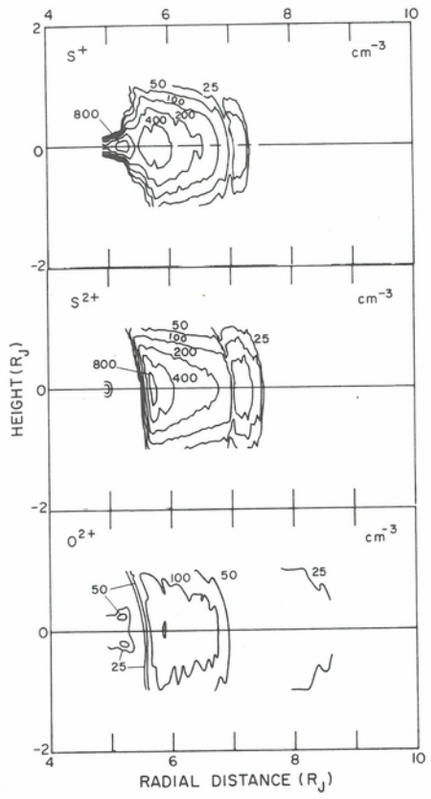

Fig. 3.8. Contour maps of the concentration of S^+, S^{2+}, and O^{2+} ions in a cylindrical coordinate system based on the centrifugal equator. The maps have been constructed from plasma measurements made along the inbound spacecraft trajectory using theoretical expressions for the distribution of plasma along dipolar magnetic field lines. The contours are in units of ions/cm^3.

Figure 3.8 shows two-dimensional concentration maps for three individual ionic species: S^+, S^{2+}, and O^{2+}. These contour maps are constructed in the same manner as in Figure 3.1. The contrast between the S^+ and S^{2+} contours shows clearly that lower ionization states (S^+) dominate the inner torus, with very little contribution from the higher ionization states. The contour map for S^{3+} ions is similar to the S^{2+} map shown here in that there are insignificant concentrations of S^{3+} ions in the inner torus. The contour map for O^+ is similar to that of S^+ in shape but with lower concentration.

Bagenal and Sullivan [1981] point out an interesting aspect of the O^{2+} contour map in Figure 3.8. The minor quantity of O^{2+} in the cold inner torus has been drawn away from the centrifugal equator by the field-aligned polarization electric field that is set up by the electrons and the heavier sulfur ions. Near 5.3 R_J, sufficient O^{2+} ions have drawn off the equator so that double maxima form in the contours approximately 0.2 R_J off the centrifugal equator, with a relative minimum at the equator itself.

In general, lighter ions of higher charge state are more easily pulled off the centrifugal equator, and thus their distribution along the field lines has a larger effective scale height. Eventually, at higher latitudes, protons must become the dominant ionic species because of their low mass relative to sulfur and oxygen (see, for example, Tokar et al. [1982]).

Present quantitative estimates of the relative abundance of the major ionic species from in situ observations should be taken as indicative, but not definitive, especially in the warm torus. In addition to the model dependencies introduced by our lack of knowledge of the thermal state of the warm torus, there are also uncertainties in the analysis due to a number of other effects. For example, all of the published analyses

Table 3.1. *Composition of the plasma in the dayside magnetosphere of Jupiter*

A/Z^*		UT:DOY R_J	64 1120 4.96	64 1016 5.3	64 0859 6.0	64 0527 8.6		64 0150 11.7	63 1550 20	63 0505 28	62 1031 42	
1	H^+							2.2	0.21[a]	0.06[a]	0.06[a]	cm^{-3}
8	O^2		48	26	160	28	20	1.5	0.10[b]	0.03[b]	0.03[b]	
					—	26[b]	9[b]					
10	S^{3+}		<5.6	<3.5	27	—	0.5	0.6	0.09[b]	0.05[b]	0.04[b]	
					170[b]	—	11[b]					
16	S^{2+}		14	39	430	—	19	2.2	0.39[d]	0.17[d]	0.10[d]	
					560[d]	16[d]	12[d]					
16	O^+		250	350	130	34	—	2.9	0.78[c]	0.35[c]	0.20[c]	
					1100[c]	32[c]	24[c]					
23	Na^+		<21	<72					0.08[b]	0.05[b]	0.02[b]	
32	S^+		91	1100	430	8	28	1.4	0.09[b]	0.07[b]		
					470[b]	11[b]	23[b]					
48	SO^+		<2	<8								
64	SO_2^+		3.5	13	73	7	7					
					8[b]	8[b]	8[b]					
	V_c		62	66	75		108	148	251	351	527	kms^{-1}
	V/V_c		1.0	1.0	1.0	1.0	0.9	0.77	0.76	0.49	0.43	

[a]Determined from low resolution spectra (McNutt, Belcher and Bridge 1981). All densities are derived from the isothermal model for the ions unless marked as follows: [b]From constant thermal speed model. [c]From constant thermal speed model when $A/Z^* = 16$ spectral peak is assumed to be all O^+. [d]From constant thermal speed model when $A/Z^* = 16$ spectral peak is assumed to be all S^{2+}.

assume that the spacecraft potential in the warm torus is zero, when in fact it is probably a few tens of volts negative. Negative potentials of this magnitude in the warm torus imply that the present analyses underestimate the concentration of the species with lower values of A/Z^*, for example, O^{2+} and S^{3+}, and overestimate the concentrations of the species with higher values of A/Z^*, for example, S^+ and S^{2+} [Bagenal, 1981]. There are similar problems associated with uncertainties in the plasma velocity in the outer parts of the warm torus (see the subsection entitled "Plasma velocities in the torus").

Finally, the assumption that the distribution functions of the ions are Maxwellian may be open to question in the warm torus, although it is demonstrably valid in the cold torus (compare Figs. 3.3 and 3.4). In particular, throughout the warm torus significant particle fluxes were detected at energies well above the bulk of the plasma. From this, Bagenal and Sullivan [1981] concluded that either very heavy molecular ions were present [Sullivan and Bagenal, 1979] or recently created sulfur ions were present that had not yet thermalized. This latter possibility is consistent with the recent analysis of ground-based observations of S^+ in terms of a hot and cold population [Brown and Ip, 1981]. There is no a priori reason to exclude such nonequilibrium distributions. A more sophisticated analysis of the in situ plasma data in the torus is in progress, and may produce quantitative differences in estimates of composition in the warm torus. However, the qualitative picture of low (higher) ionization states in the cold (warm) torus is well established, and in good agreement with other spacecraft and ground-based measurements [see Bagenal, 1981].

Minor ionic species. In addition to the major ionic species, there is at times clear evidence for various minor species, such as the peak at an A/Z^* value of 64 (probably SO_2^+) in Figure 3.3. When the presence of the minor species is indicated by a distinct peak or shoulder, we give a quantitative estimate of its concentration in Table 3.1. When there is no clear indication of the presence of a given minor ion, we place an upper limit on its concentration, as indicated in Table 3.1 and illustrated in Figure 3.3 for Na^+ and SO^+.

The well-resolved spectral peaks at A/Z^* values of 23 found in cold regions of the middle magnetosphere suggest sodium ions form about 10% of the ionic composition there. In the inner torus filling the gap between the peaks at A/Z^* values of 16 and 32 with appropriate amounts of ions with A/Z^* values of 23 suggests sodium is relatively less abundant closer in, forming less than $\sim 5\%$ of the ion composition. If the spectral feature at A/Z^* values of 64 is SO_2^+, then, in the cold torus, its concentration is $\sim 1\%$ of the total ion concentration. In the warm torus, the concentration of SO_2^+ near Io's orbit is $\sim 1\%$ of the total for the common thermal speed model and $\sim 5\%$ of the total for the isothermal model.

In the middle magnetosphere, protons comprise up to $\sim 30\%$ of the number density with their importance increasing with distance away from the plasma sheet, as discussed in the subsection entitled "The plasma sheet." In the inner magnetosphere the kinetic energy of H^+ is generally below the energy-per-charge threshold of the plasma instrument. However, there are a few spectra before closest approach with a feature in the lowest channels that might be the tail of a distribution function below the well-resolved spectral peak at an A/Z^* value of 8. If this feature corresponds to H^+ (He^{2+}) ions with the same temperature as the heavy ions, then a fit to the data gives concentration estimates of 3% (0.4%) of the total ion population. Although these percentages should be regarded with caution (because the observed distribution does not include the peak), their low values are consistent with the good agreement in the torus between

Table 3.2. *Vector velocities in the cold torus as seen in the corotating frame*[a]

Time UT on March 5, 1979	Distance R_J	Corotation speed (km/s)	$\mathbf{V}\cdot(\hat{\mathbf{r}}\times\hat{\mathbf{b}})$ / $\lvert\hat{\mathbf{r}}\times\hat{\mathbf{b}}\rvert$ ~ Azimuthal	$\mathbf{V}\cdot(\hat{\mathbf{b}}\times(\hat{\mathbf{r}}\times\hat{\mathbf{b}}))$ / $\lvert\hat{\mathbf{r}}\times\hat{\mathbf{b}}\rvert$ ~ Radial	$\mathbf{V}\cdot\hat{\mathbf{b}}$ ~ Southward
1016	5.28	66.3	−0.1	−0.9	1.4
1120	4.95	62.1	−0.1	−0.7	1.7

[a] After Table 2 of Bagenal [1981]

the electron concentration from the Planetary Radio Astronomy experiment and the elementary-charge concentration of positive ions with $A/Z^* \geq 8$ (see the subsection entitled "Elementary-charge concentrations in the torus"). The fact that protons are a major ion by number in the middle magnetosphere but apparently a minor ion in the torus may be indicative of the source – for example, the H^+ ions might originate in the Jovian ionosphere, or perhaps from the icy Galilean satellites.

Plasma velocities in the torus

In the cold inner torus, corotating flow is essentially parallel to the symmetry axis of the main sensor cluster, and the various ionic species are cold enough so that the response of each of the Faraday sensors can be reliably taken to be a constant. In such a situation, the full vector velocity can be reconstructed with high accuracy from the simultaneous measurements in the A, B, and C sensor [Bridge et al., 1977]. For example, consider the C sensor data at 1016 UT on March 5, 1979 (Fig. 3.3). Data from the A and B sensors are similar, and each of the three sensors can be used to determine on independent component of the full vector velocity. Although the three velocity components so determined are not orthogonal, it is a simple matter to reconstruct the orthogonal components from them. In Table 3.2, we give two determinations of the vector velocity in the cold torus, from Bagenal [1981], based on simultaneous fits to all three sensors. These velocity components are quoted in the corotation frame of reference (i.e., after subtraction of rigid corotation from the inertial velocity). The unit vector $\hat{\mathbf{b}}$ is the local magnetic field direction as determined by the magnetometer experiment [Ness et al., 1979a], and the velocities are resolved into a coordinate system based on $\hat{\mathbf{b}}$ and the unit vector in the radial direction $\hat{\mathbf{r}}$. From Table 3.2, we see that the plasma in the cold torus moves at the corotational velocity to within a few kilometers per second. The probable error in the determination of this velocity is of the same order, so that there is no evidence for any systematic deviation from strict corotation in the cold torus.

In the warm torus, it is more difficult to determine full vector velocities, both because the plasma is warmer, and because the flow is more oblique to the A sensor normal. However, estimates of the velocity component into the C sensor are still reasonably straightforward. These estimates are consistent with strict corotation in the inner part of the warm torus, although there is some indication that the flow falls below corotation at the outer boundary of the warm torus [Bagenal and Sullivan, 1981]. This result is in keeping with the Planetary Radio Astronomy observations of Kaiser and Desch [1980], who find evidence for subcorotation of the plasma flow by 3% to 5% near 8 R_J, and it foreshadows the striking deviations from strict corotation found in the middle magnetosphere (see the subsection entitled "Plasma velocities in the middle magnetosphere").

Comparison with the Pioneer 10 plasma observations

Heavy-ion dominance of the Jovian magnetospheric plasma is a relatively new concept. In particular, all of the initial results of the Pioneer particle experiments were interpreted in terms of light ions. With the advantage of hindsight, it is worth reconsidering the results of Frank et al. [1976] in light of current views. In the Pioneer 10 data in the inner magnetosphere, positive-ion flux density vs. energy-per-charge spectra showed peaks well above the corotation energy for protons. With the assumption that the plasma was entirely composed of protons, Frank et al. [1976] concluded that the plasma was subsonic and analyzed the Pioneer 10 data accordingly. It now seems plausible that instead of hot, subsonic protons, the Pioneer 10 experiment was detecting transonic or supersonic heavy ions. For example, at 2.85 R_J, Frank et al. [1976] found a characteristic energy per charge of 105 V compared to corotational energies per charge of only 6.5 V for protons. However, heavy ions with mass-to-charge ratios around 16 would have corotational energies per charge of 100 V at this distance and thus could account for the observed energy-per-charge spectrum with no need for a hot proton component. This suggestion that Pioneer 10 detected heavy ions from Io is not a new one, and has been previously postulated by Hill and Michel [1976], Neugebauer and Eviatar [1976], and Goertz and Thomsen [1979b].

Intriligator and Miller [1981] have recently reexamined the Pioneer 10 positive-ion data between 5.4 and 6.9 R_J, and their results give additional weight to these earlier suggestions. Among other findings, these authors present evidence for the corotating ions S^{2+} and O^{2+}, with temperatures of tens of eV. The plasma current profile shows a relative variation with distance which is qualitatively similar to the density profile shown in Figure 3.7. There is a well-defined maximum at ~ 6 R_J (as contrasted to the 5.7 R_J maximum for Voyager), with a steep fall-off toward Jupiter and a gradual decrease away from Jupiter. Although Intriligator and Miller [1981] do not give estimates of ion concentrations, the concentrations quoted by Frank et al. [1976] are qualitatively consistent with the Voyager results, if allowance is made for the A/Z^* dependence of the estimates (the interpretation as protons underestimates the true concentration of heavy ions). These similarities between Pioneer 10 and Voyager 1 observations are evidence for the presence of an Io torus in December of 1973 with many of the properties of the torus as observed in March of 1979. Quantitative comparisons of the two data sets may provide insight into the long-time-scale variability of the torus.

3.3. The Io flux tube

Velocity perturbations near the flux tube

The nature of the direct interaction of Io with the magnetospheric plasma is an area of long-standing interest in space plasma physics. For this reason, Voyager 1 was targeted for passage through the Io flux tube at some 20500 kilometers south of Io. The subsequent Voyager 1 measurements of the perturbations in the magnetic field and in the fluxes of low-energy positive ions near the Io flux tube clearly established the presence of a large amplitude Alfvénic wave pattern propagating southward along the magnetic field lines [Ness et al., 1979a; Neubauer, 1980; Acuña, Neubauer, and Ness, 1981; Belcher et al., 1981]. The close correlation between the magnetic field and ion-flux-density perturbations near Io is shown in Figure 3.9. The ion flux density in this figure is from the B sensor of the main cluster. All sensors in the main cluster exhibited this same increase in flux density near the flux tube, closely correlated with the magnetic field perturbation.

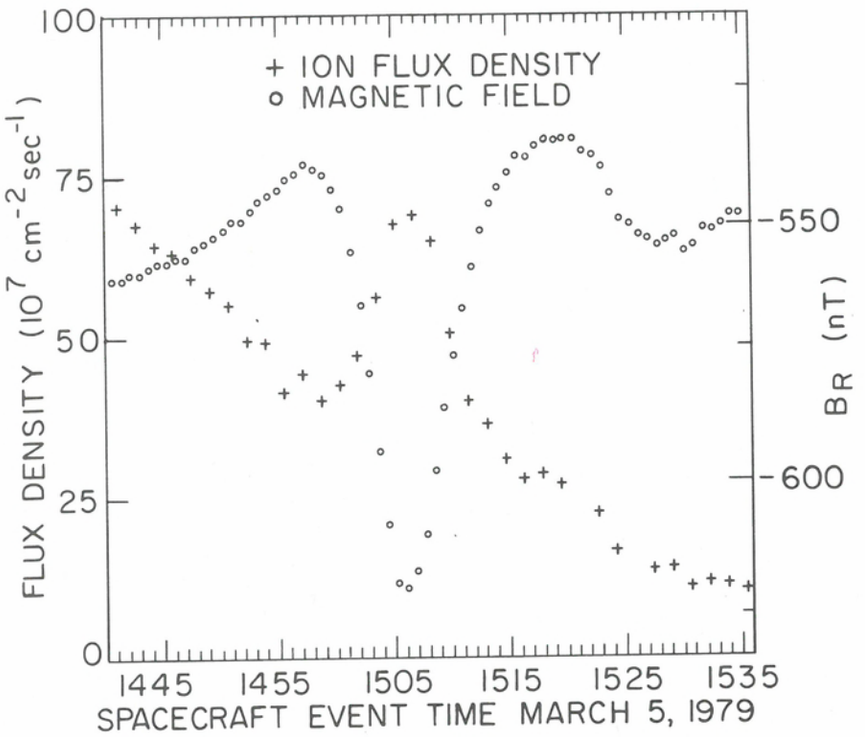

Fig. 3.9. Plots of the ion flux density from the B sensor and of the radial component of magnetic field as a function of time near the Io flux tube. The close anticorrelation between these two measurements indicates southward propagation of the Ionian Alfvén wave.

Figure 3.10 is a schematic illustration of the probable flow pattern sampled by the spacecraft. The location of the flux tube relative to the spacecraft trajectory is determined by fits to the magnetic field measurements [Acuña, Neubauer, and Ness, 1981]. If Io is a good conductor, the flow pattern of the ambient plasma external to the flux tube should be similar to incompressible flow around a cylinder [Scholer, 1970]. Streamlines for such a flow are illustrated in Figure 3.10. We indicate in this figure the cone on which the normals to the sensors in the main cluster lay, and also the time of the maximum in the flux density perturbation shown in Figure 3.9 (1506 UT on March 5, 1979).

The interpretation of the Plasma Science observations is straightforward in the context of this flow pattern. The perturbation in both field and plasma parameters occurred as the ambient magnetospheric plasma deviated from strict corotation to flow around the Io flux tube, so as to avoid the plasma "frozen" to the field lines threading Io. At the closest approach to the flux tube, this deviation from corotation was such as to bring the flow more nearly into the main cluster, thus increasing the ion flux density into the main cluster sensors. The anticorrelation between the radial component of the field and the flux density perturbations indicated southward propagation of the pattern [Belcher et al., 1981]. This qualitative interpretation can be made quantitative by an analysis of the multisensor data for oblique angles of incidence (see the subsection

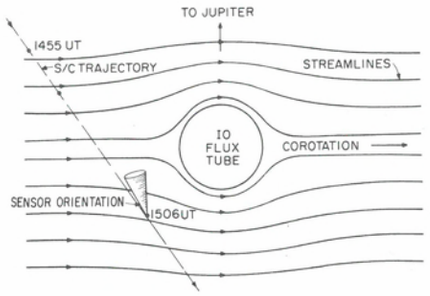

Fig. 3.10. The Voyager 1 trajectory with respect to the Io flux tube looking down from the north. The streamlines are for incompressible flow around a cylinder. The cone indicates the orientation of the main sensor normals.

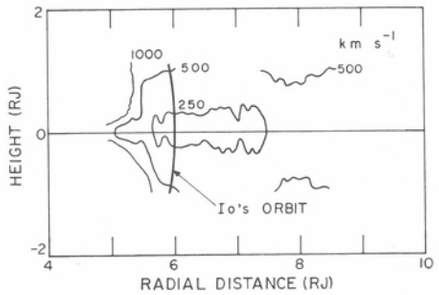

Fig. 3.11. A contour map of local Alfvén speed calculated from the O4 magnetic field model [Acuña and Ness, 1976c] and the total ion mass density, measured along the spacecraft trajectory and extrapolated along the magnetic field lines.

entitled "Plasma velocities in the middle magnetosphere"), and such a study is in progress (Barnett and Olbert, private communication, 1981).

Alfvén speeds in the torus

Bagenal and Sullivan [1981] have constructed contours of constant Alfvén speed for the Io torus, using their two-dimensional model for the total mass density of the plasma and the O4 model of Acuña and Ness [1976c] for the magnetic field configuration. This contour map is shown in Figure 3.11. Although the calculated local Alfvén speed everywhere exceeds the local corotation speed, it displays a region of uniformly low values in the outer torus with minimum speeds of $\lesssim 250$ km s^{-1} occurring near the centrifugal equator. The position of Io with respect to the centrifugal equator also varies as shown in Figure 3.11. The Alfvén speed of the plasma in the vicinity of Io therefore varies by a factor of two with the System III longitude of the satellite. The large Alfvén speeds outside the torus mean that the time for Alfvén waves generated near Io to reach the ionosphere is largely determined by the length of the propagation path in the torus. This transit time is therefore modulated by the System III position of Io. Similarly, other properties of the propagating waves, such as geometry and damping, will also vary with longtitude. The subsequent changes in the field-aligned current associated with the Alfvén wave may explain the Io-modulation of the decametric radiation [Gurnett and Goertz, 1981].

3.4. The middle magnetosphere

General morphology

As we move into the middle magnetosphere (between ~ 10 and $\sim 40\ R_J$), the dominant plasma structure becomes the concentration enhancements associated with crossings of the plasma sheet. Because of the increasing plasma velocity with increas-

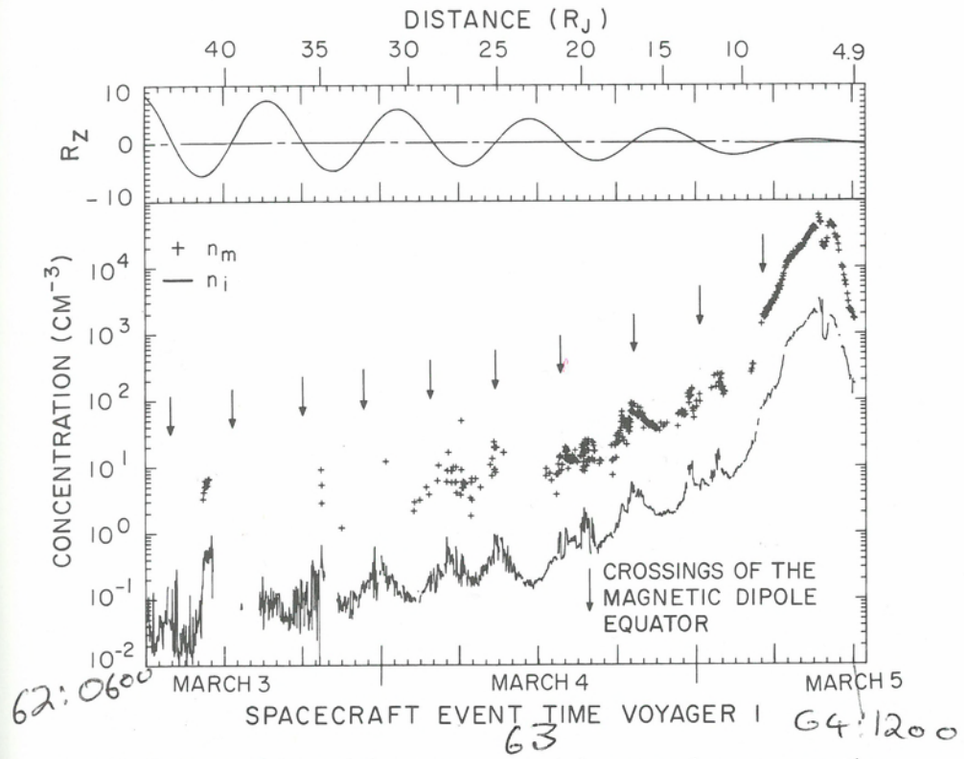

Fig. 3.12. Estimates of the total elementary-mass and elementary-charge concentrations of positive ions, n_m and n_i, in units of amu per cm^3 and elementary charges per cm^3, respectively, for the Voyager 1 encounter. The top panel shows the distance of the spacecraft from the magnetic dipole equatorial plane and arrows in the bottom panel indicate the crossings of this plane. Dates are given at 1200 UT.

ing distance, H^+ moves into the energy range of the Plasma Science instrument. Figure 3.12 shows values of the elementary-charge concentration n_i for positive ions with energy per charge between 10 and 5950 V, for the inbound Voyager 1 trajectory [McNutt, Belcher, and Bridge, 1981]. These elementary-charge concentrations are obtained by taking the total flux density of positive charge for the sensor that is least oblique to corotating flow and dividing by a model velocity component into that sensor (see the subsection entitled "Plasma velocities in the middle magnetosphere"). Such an estimate of n_i can be obtained for every positive ion spectrum, regardless of whether the various ionic species are resolved, and thus the n_i curve is essentially continuous except for data gaps. Simultaneous estimates of n_e, the total electron concentration, can be obtained from the electron measurements, and in the middle magnetosphere the estimates of n_i and n_e show good agreement [Scudder, Sittler, and Bridge, 1981]. Figure 3.12 also gives values of the positive-ion elementary-mass concentration n_m as obtained from fits of Maxwellians to the energy-per-charge spectra of positive ions. As discussed in detail by McNutt, Belcher, and Bridge [1981], in the middle magnetosphere we require for such fits a proton peak that is well resolved from the heavy ion peak in the positive-ion spectra. Frequently the ions are of sufficiently low Mach number that the protons and the heavy ions are not well resolved, especially at larger radial distances, so fit estimates of n_m and the ion temperature cannot be obtained for every

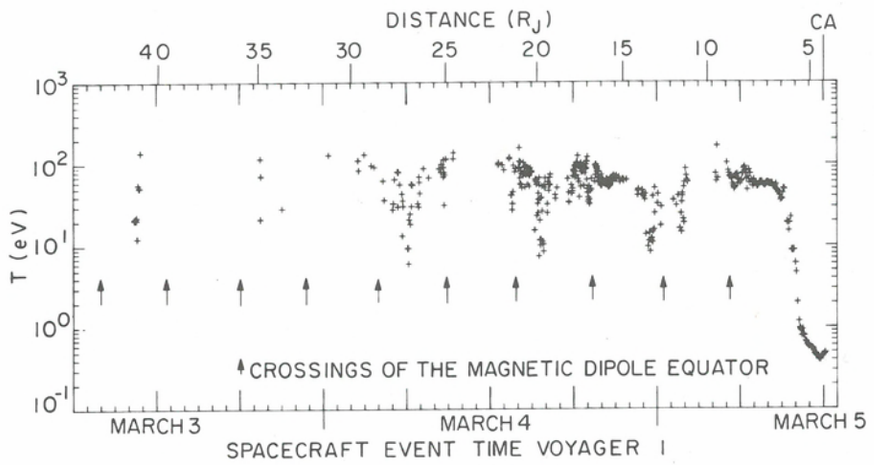

Fig. 3.13. Positive ion temperatures for Voyager 1 inbound from Bagenal and Sullivan [1981] and McNutt, Belcher, and Bridge [1981]. The time period covered is the same as that in Figure 3.12.

spectrum, as is obvious from the coverage in Figure 3.12. Resolved spectra tend to occur at local maxima in concentration, because the ions are cooler there.

The concentration profiles in Figure 3.12 are dominated by the Io plasma torus in the inner magnetosphere, with a rapid decrease in concentration as we move into the middle magnetosphere. Superimposed on this overall decrease are two local increases every Jovian rotation period (9 hr 55 min.), with the local maxima near crossings of the magnetic-dipole equatorial plane. The local increases occur as the plasma sheet sweeps across the spacecraft twice each planetary rotation period. These increases in concentration are accompanied by marked decreases in the temperatures of both positive ions and electrons. For example, Figure 3.13 shows the available positive ion temperatures from fits to ion spectra, over the same time period as covered in Figure 3.12. A close examination of the two figures shows that the local maxima in concentration are associated with local temperature minima on Voyager 1 inbound.

On Voyager 2 inbound, the plasma sheet crossings are not as clearly defined. Figure 3.14 shows the positive-ion concentrations from the middle magnetospheric passage of Voyager 2, in a format similar to Figure 3.12. The smaller number of estimates of n_m as compared to Voyager 1 reflect a smaller number of positive-ion spectra in which the protons are well resolved from the heavy ions. This lack of resolution is due to an overall decrease in the Mach number of the flow on Voyager 2 inbound, which we could attribute to an increase in temperature, but is more likely due to a decrease in flow velocity during the Voyager 2 encounter (see the subsection entitled "The breakdown of corotation"). Before approximately 1400 UT on July 8, 1979 ($\sim 25\ R_J$ inbound), concentration peaks near crossings of the magnetic equatorial plane are reasonably well defined. After this time on the inbound trajectory, there were no well-defined peaks near the crossings, except for the peak near closest approach, at $\sim$2100 UT on July 9. In part, the Ganymede associated dropouts centered at 15 R_J [Burlaga, Belcher, and Ness, 1980; Connerney, Acuña, and Ness, 1981] may obscure some of the plasma sheet increases. However, the lack of pronounced crossings after $\sim$1400 UT on July 8, probably reflects a thickening of the dayside plasma sheet due to the arrival of a solar wind pressure ridge on July 8. The increase in upstream solar wind pressure begins at

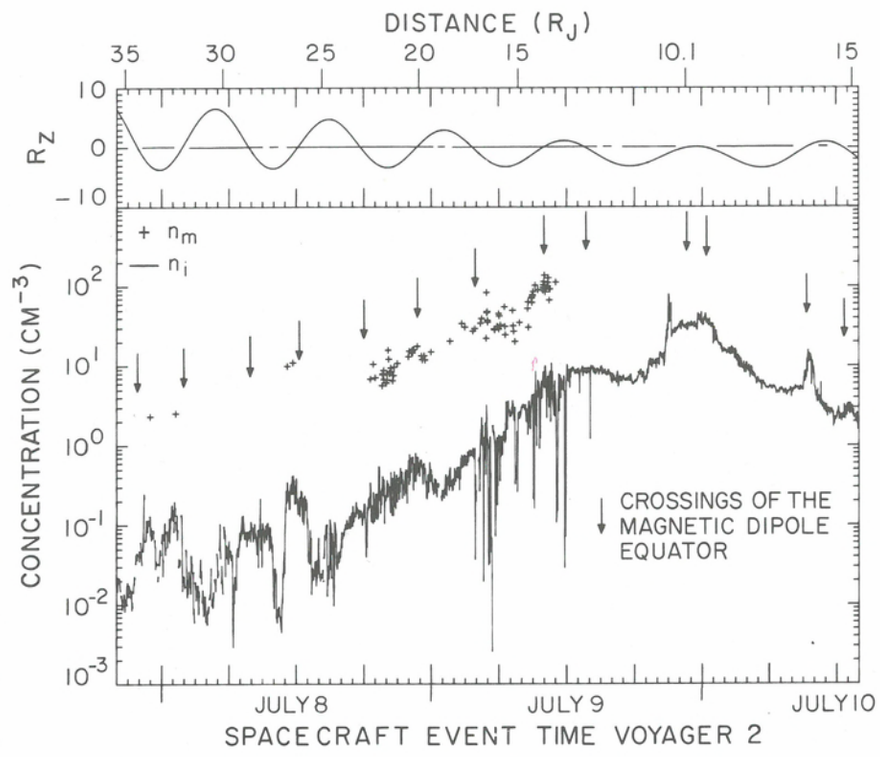

Fig. 3.14. Estimates of the total mass and charge concentrations of positive ions for the Voyager 2 encounter, similar in format to Figure 3.12.

approximately 1800 UT on July 7 rising from a value of $\sim 4 \times 10^{-11}$ N/m^2 to a peak of $\sim 27 \times 10^{-11}$ N/m^2 at $\sim$1200 UT on July 8, with a slow decrease over the next three or four days. Using a scaling law inversely proportional to the cube root of the pressure, Goodrich, Sullivan, and Bridge [1980] find that the standoff distance to the Jovian bow shock should have decreased from ~ 107 to $\sim 58\ R_J$ over this period. This overall compression of the magnetosphere probably leads to a thickening of the plasma sheet on the dayside, as has been previously suggested on the basis of Pioneer energetic particle data [MacDonald, Schardt, and Trainor, 1979]. There are also suggestions in the data that the solar-wind compression may cause plasma flows away from the dayside current sheet, as discussed in the subsection entitled "Nonazimuthal flows."

Even when well-defined concentration maxima occur near crossings of the magnetic equatorial plane, we note that crossings of the plasma sheet (as defined by the plasma-concentration signature) do not necessarily coincide with crossings of the current sheet (as defined by the magnetic field signature). The most prominent example of this distinction between plasma sheet and current sheet is the bifurcated plasma sheet crossing near 0000 UT on March 5, at 13 R_J. Figure 3.15 shows the high resolution positive-ion spectra during this crossing, from 2200 UT on March 4 to 0215 UT on March 5, 1979. The peaks in relative flux density in this figure correspond to the peaks in concentration. The anticorrelation between concentration and temperature is readily apparent (see also Figs. 3.12 and 3.13). Of the two peaks in the concentration profile, one peak is north of the expected crossing of the magnetic dipole equatorial plane, at 4.0° in magnetic latitude (2330 UT on March 4), and one peak is distinctly south of the expected

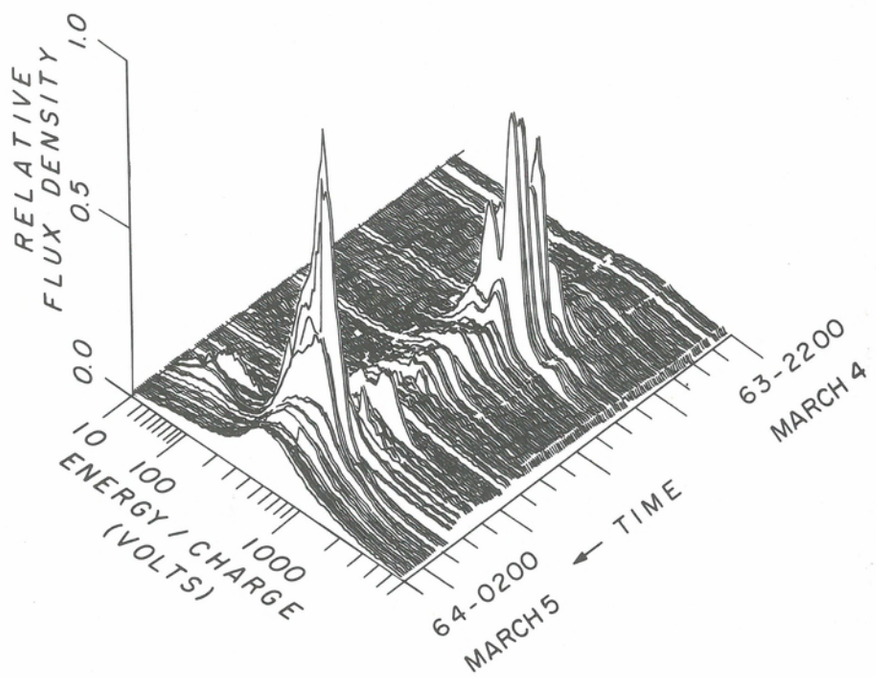

Fig. 3.15. The relative flux density of positive ion charge vs. energy per charge as measured in the D sensor between 2200 UT on March 4 and 0215 UT on March 5. The two main peaks in the prominent ion spectra near 2330 UT are due to ions with A/Z^* ratios of 10.67 (S^{3+}) and 16 (S^{2+} or O^+), with a much smaller peak above the 16 peak at an A/Z^* value of 32 (S^+). The cold peaks around 2330 UT on March 4 occur near a magnetic dipole latitude of $+4.0°$, whereas the cold peaks around 0139 UT on March 5 are at $-7.9°$ magnetic latitude. The current sheet crossing is at 0000 UT on March 5 near 1.3° magnetic dipole latitude.

crossing, at $-7.9°$ magnetic latitude (0139 UT on March 5). The current sheet crossing, as defined by the change in the poloidal field direction from away to toward the planet, occurred close to the dipole equatorial plane, at 1.3° magnetic dipole latitude (0000 UT on March 5 [Connerney, Acuña, and Ness, 1981]). The crossing near 21 R_J on Voyager 1 inbound is somewhat similar, in that there is a peak in concentration near the crossing of the magnetic dipole equatorial plane, close to but not exactly centered on the current sheet crossing at 1405 UT on March 4, near 0° magnetic dipole latitude. In addition, there is a more pronounced increase in concentration, 7.1° south of the expected crossing, at 1530 UT on March 4, far from the current sheet crossing (see Fig. 3.12). Figure 25 of McNutt, Belcher, and Bridge [1981] shows the high-resolution positive-ion spectra during this crossing. Again, the increases in ion concentration are accompanied by pronounced decreases in ion temperature by as much as a factor of 10 (from ~ 100 to ~ 10 eV, see Fig. 3.13).

The plasma sheet

With the caveat that the plasma sheet and the current sheet do not always coincide, we examine in detail both the electron and positive ion structure of a sheet crossing near 17 R_J on Voyager 1 inbound, for which the plasma and current sheet signatures do, in

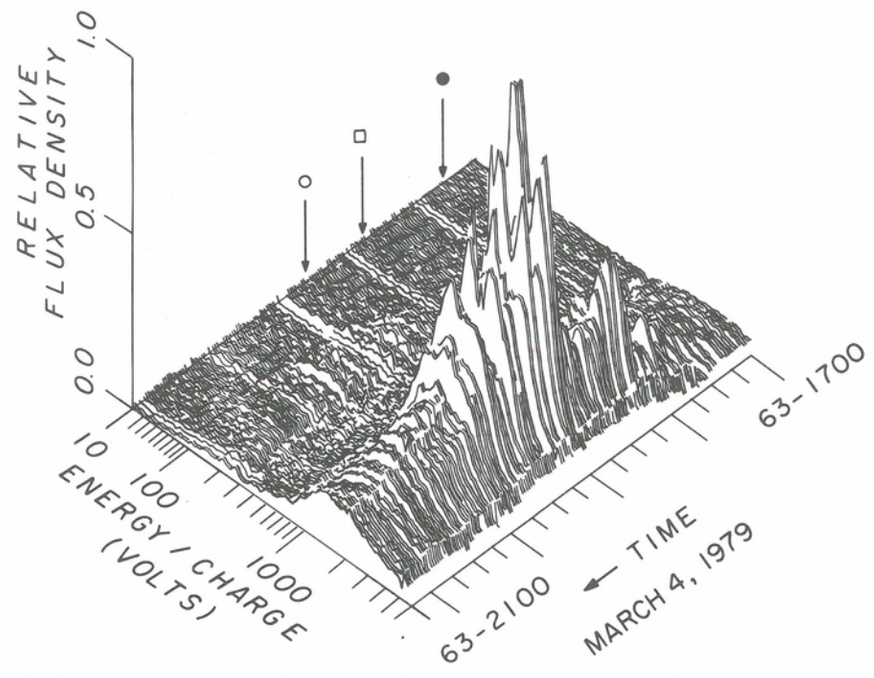

Fig. 3.16. The relative flux density of positive-ion charge as measured in the D sensor between 1700 UT and 2115 UT on March 4, 1979, similar in format to Figure 3.15. The arrows mark the times of the three electron spectra shown in Figure 3.17.

fact, coincide. Although the cooling effect in the positive ions is not as pronounced as during other crossings, the ion spectra show enough resolution throughout the crossing for detailed quantitative analysis. Figure 3.16 shows the high-resolution positive-ion spectra during this crossing, from 1700 UT to 2115 UT on March 4. The heavy-ion species occupy the energy-per-charge scan from ~ 600 to ~ 4000 V. The increase in concentration and decrease in temperature which defines the sheet crossing are apparent. The dominant cold peak near 1900 UT in this figure is due to S^{3+}. The proton signal is lost in the noise in the high-resolution ion spectra, but it is clearly present in the low resolution spectra. Electron distribution functions at three different locations in the sheet (at the times indicated by arrows in Fig. 3.16) are shown in Figure 3.17. The electron spectrum at 1723 UT (filled circles) is representative of spectra away from the sheet crossing; the spectrum at 1906 UT (open circles) occurs at the peak concentration in the crossing; the spectrum at 1824 UT (open boxes) occurs during a subsidiary density enhancement south of the main peak. As in the inner magnetosphere (see Fig. 3.6), the electron distribution functions exhibit a cold, thermal component as well as a higher-energy, suprathermal component. It is qualitatively clear from Figure 3.17 that the concentration increase in the current sheet is due primarily to an increase in the concentration of the core electrons, accompanied by a simultaneous decrease in their temperature.

Figures 3.18 and 3.19 display quantitative plasma parameters for both electrons and positive ions in this crossing, as well as magnetic field parameters from Ness et al. [1979a]. The bottom panel of Figure 3.18, as well as the second panel from the top of the figure, refer to positive-ion velocities, which will be discussed in the subsection entitled "Plasma velocities in the middle magnetosphere." The second panel from the bottom

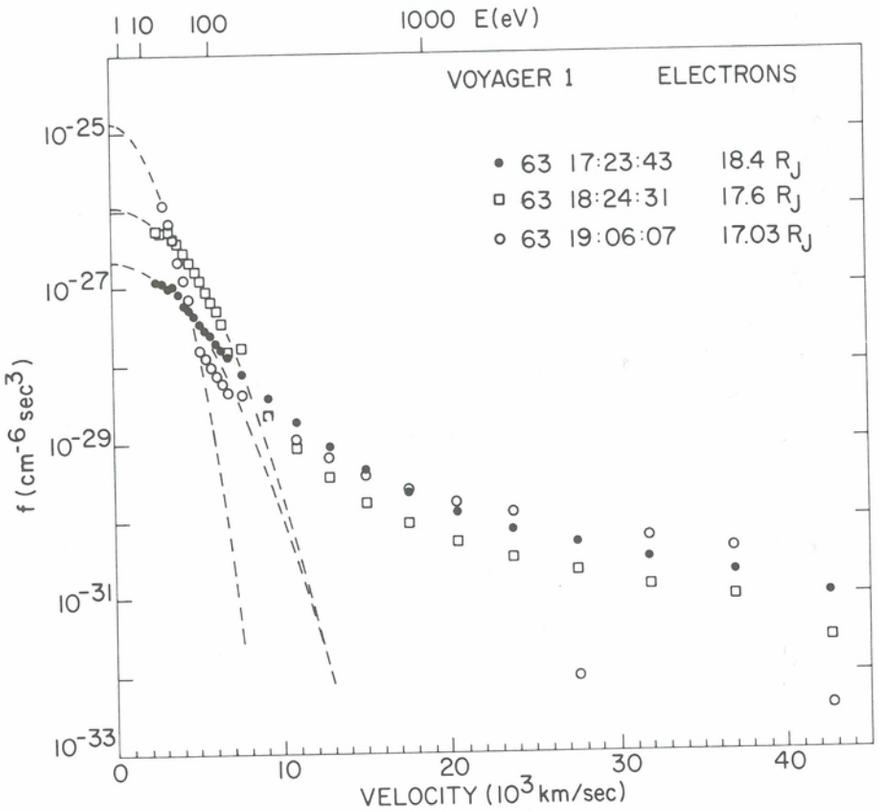

Fig. 3.17. Electron distribution functions vs. electron speed during the Voyager 1 inbound plasma sheet crossing near 17 R_J. For reference, the corresponding electron energy in eV is given at the top of the figure. The spectra are from the times indicated by arrows in Figures 3.16 and 3.19. Gaussian fits to the cold "core" electron component are indicated by the dashed lines.

of Figure 3.18 gives estimates of n_m (in amu/cm^3) obtained from fits to positive-ion spectra with resolved ion species, when available. The middle panel of the figure shows the ratio of total elementary-mass concentration to that of the protons, n_p. The top panel shows the temperature of the protons (triangular), which McNutt, Belcher, and Bridge [1981] found to be a good measure of the heavy-ion temperatures, and also the temperature of the core electrons (crosses), obtained from Maxwellian fits to the thermal electron component. In Figure 3.19, the top panel displays the total electron number density n_e obtained from integration of the full electron distribution function. Also shown is the halo number density n_H, obtained by direct integration over the full distribution function minus the Maxwellian fit to the core. In the second panel from the top, T_e is the mean energy of the electrons as obtained by direct integration over the observed distribution function, T_C is the temperature of the core electrons from the Maxwellian fit, and T_H is the characteristic energy of the halo electrons as determined from partial pressures. Also displayed in Figure 3.19 are the magnetic field strength, two direction angles of the field, and the Pythagorean variance as determined from 48 s averages.

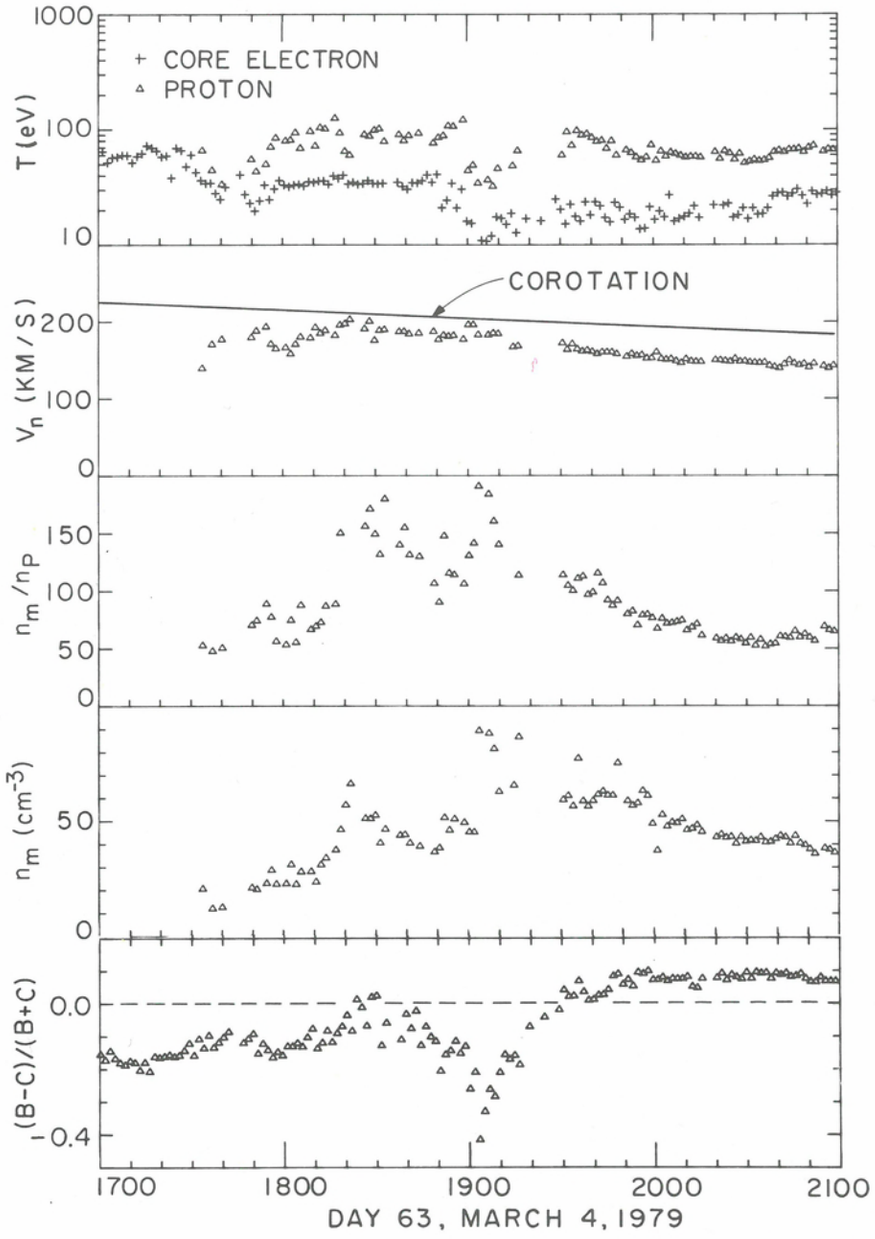

Fig. 3.18. A plot of plasma parameters for the plasma sheet crossing near 17 R_J on Voyager 1 inbound, corresponding to the time interval shown in Figure 3.16.

From the detailed analysis of this and other current sheet crossings in the middle magnetosphere, Scudder, Sittler, and Bridge [1981] and McNutt, Belcher, and Bridge [1981] conclude that:

1. The plasma sheet concentration maxima are routinely cooler than their surroundings, with respect to both electrons and positive ions. There is a tendency for the more abrupt crossings to exhibit lower ion temperatures.

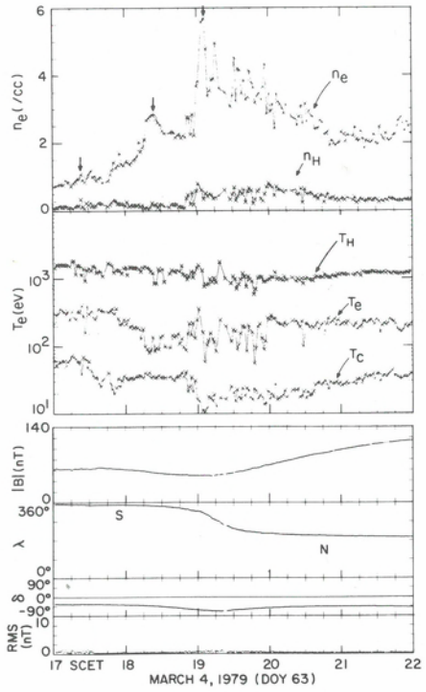

Fig. 3.19. A plot of electron and magnetic field parameters for the plasma sheet crossing near 17 R_J on Voyager 1 inbound, corresponding to the time intervals shown in Figures 3.16 and 3.18.

2. The heavy ions are greatly enhanced with respect to protons in the plasma sheet, presumably because of the larger scale height of the lighter protons. Both in and out of the sheet, the protons are essentially negligible in terms of total elementary-mass concentration (~2% or less), at least over the limited range of magnetic latitudes sampled by the Voyager spacecraft.
3. At the center of the crossing of the plasma sheet by Voyager 1 at 17 R_J (see Figs. 3.18 and 3.19 near 1900 UT), $\rho V_n^2/2$ exceeds the magnetic energy density by about a factor of three – that is, the flow has become super-Alfvénic in the sheet owing to the high concentrations and low field strengths. Away from the maximum sheet density, where the mass concentration is lower and the magnetic field strength higher, the flow is sub-Alfvénic. As we move outward from this 17 R_J crossing on the dayside in the Voyager 1 encounter, every subequent sheet crossing shows this transition from sub-Alfvénic to super-Alfvénic flow. As we move inward from this crossing, the flow is always sub-Alfvénic. Thus, on Voyager 1, the Alfvénic critical point in the plasma sheet must occur inside of 17 R_J. Note that the Alfvénic Mach number exceeds unity in the sheet maxima beyond 17 R_J on Voyager 1 without any drastic consequences, in accord with theoretical conclusions [Goldstein, 1977; Goertz, 1979]. On Voyager 2, however, the sheet crossings for which we have mass concentration estimates do not tend to show super-Alfvénic velocities. We attribute this difference to lower azimuthal velocities on the Voyager 2 pass (see the subsection entitled "Plasma velocities in the middle magnetosphere"), and to the lack of large concentration enhancements in the plasma sheet between ~12 and ~25 R_J, as discussed in the subsection entitled "General morphology."
4. The enhancement in the total electron concentration in the sheet is due to an increase in the concentration of the thermal population; the suprathermal density

enhancement is less pronounced, and is nearly symmetric about the magnetic equator.
5. The reduction in the mean electron temperature T_e is due predominantly to a decrease in the core temperature T_C, with the suprathermal energy T_H relatively unaffected. Scudder, Sittler, and Bridge [1981] suggest that the suprathermal population observed within the plasma sheet is a global population that is not especially confined to the vicinity of the sheet. By contrast, the thermal population is localized by the presence of the heavy ions, and by the consequent large polarization potential of the order of the mean electron energy they must overcome to leave the sheet.
6. The mean electron temperature T_e is asymmetric about the plasma sheet, being on average cooler on the centrifugal side of the sheet (the generally positive Jovigraphic latitude of the spacecraft implies that the centrifugal equator will be encountered south of the magnetic dipole equator). Steady-state arguments imply that cooler plasma should be found toward the centrifugal equator and hotter plasma toward the magnetic equator [see Appendix B, and Hill, Dessler, and Michel, 1974; Goertz, 1976; Cummings, Dessler, and Hill, 1980]. In some average sense, this is the pattern observed in the electron parameters by Scudder, Sittler, and Bridge [1981], both in the middle and outer magnetosphere.
7. The fraction of suprathermal electrons in the plasma sheet increases with increasing Jovicentric distance, from $\lesssim 1\%$ in the torus, to ~10% at ~15 R_J, to ~50% at ~40 R_J. As a consequence, the mean electron temperature in the sheet proper increases with increasing Jovicentric distance. Scudder, Sittler, and Bridge [1981] envisage this positive temperature gradient as due to the intermixing of a cool, dense plasma that is transported directly outward from the Io torus without diversion from the centrifugal equator and a hot suprathermal bath of electrons at midlatitudes, which is an older and possibly recirculated population (with possibly an ionospheric component). As the cool plasma become more dilute at greater distances, the suprathermal bath of electrons increasingly dominates the number density of electrons in the sheet proper.
8. The sonic Mach number of the positive ions decreases with increasing radial distance, presumably owing to an increasing temperature. There is some evidence for this in the ion temperature estimates of Figure 3.13, but a stronger argument involves the lack of resolved proton/heavy-ion peaks at larger distances. A Mach-one proton distribution with a bulk speed of 200 km/s has a temperature of ~200 eV, and it will not be resolved from the heavy-ion signature. Gaps in the temperature profile in Figure 3.13 are due to a selection effect related to temperature, because we have only analyzed spectra with resolved proton peaks for this figure. Thus, we have systematically eliminated ion spectra exhibiting temperatures greater than ~200 eV, and the large number of gaps at greater radial distances implies an increased incidence of hotter ion spectra. If we relax the requirement that a resolved proton peak be present, and fit all low-resolution ion spectra, we qualitatively find that within 40 R_J the ion temperature is typically ~1 keV or less. This estimate reflects the fact that in almost all cases, the distribution functions of the measured spectra peak below 6 keV, a result that is consistent only with a plasma temperature of less than ~6 keV.
9. Even at ~15 R_J where the suprathermals are ~10% by number in the sheet proper, Scudder, Sittler, and Bridge [1981] find that the suprathermals account for the majority of the electron energy density ($\gtrsim 75\%$) in the sheet. That is, the thermal population dominates the number density, and the suprathermal population, the energy density.

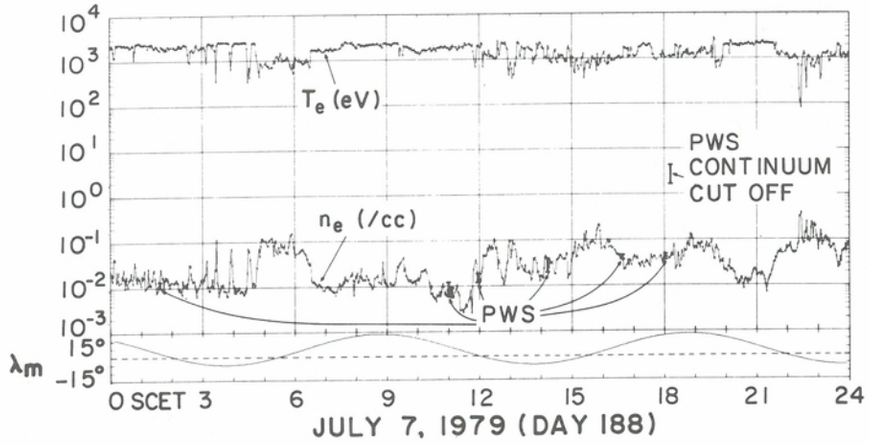

Fig. 3.20. Time series day plot of Voyager 2 inbound electron parameters on July 7, 1979, when the spacecraft is between 46 and 33 R_J from Jupiter. In the top panel, the Plasma Science determination of n_e and T_e are displayed. In addition, the Plasma Wave Science broadband continuum cutoff determinations of the electron concentration are indicated by the symbol *I*. In the next panel down, the tilted dipole magnetic latitude of the spacecraft λ_m in degrees has been added for reference, where the dashed horizontal line indicates when the spacecraft passed the magnetic dipole equator.

10. The plasma pressure at the sheet crossings due to both ions and electrons in the energy range of the Plasma Science experiment is insufficient to balance the decrease in magnetic pressure. If the plasma sheet is in quasistatic equilibrium, pressure balance must be caused by ions with energies above the energy per charge range of 6 kV of the Plasma Science experiment, consistent with the results of Krimigis et al. [1981] and Lanzerotti et al. [1981] (see Chapter 4). It is tempting to speculate that the ion distribution functions have both a thermal and suprathermal component, as do the electrons, perhaps for similar reasons. In particular, the suprathermal ion component may dominate the ion pressure even though it may not dominate the concentration as suggested by Belcher, Goertz, and Bridge [1979]. However, we also note that there may be severe problems with the quasistatic approximation, at least for some of the dayside current sheet crossings, particularly those on Voyager 1 inbound at 13 and at 21 R_J. It is hard to understand how any quasistatic model of the plasma sheet could produce mass concentration peaks north and south of the field reversal region, with a relative minimum at the reversal.
11. Even in the outer parts of the middle magnetosphere, the anticorrelation between n_e and T_e is a pronounced effect. This is illustrated in Figure 3.20, which displays electron parameters from 46.5 to 33.1 R_J (July 7) on Voyager 2 inbound. Note especially from 0200 UT to 0500 UT of July 7, the "spikey" appearance and disappearance of an electron plasma that is much cooler and denser than the surrounding regions. These cool electron concentration enhancements are well correlated with depressions in the magnetic field strength; they may represent phenomena associated with the proximity of the plasma sheet. The broader concentration increases in Figure 3.20 are, of course, associated with expected current sheet crossings. Note, however, that even within these broad increases, there are local spikes in concentration containing cool electrons (e.g., the spikes in crossing near 2230 UT on July 7 in Fig. 3.20). These spikes appear to be uniformly distributed in magnetic latitude within the sheet, and lead to a sheet structure that is complex and highly time variable.

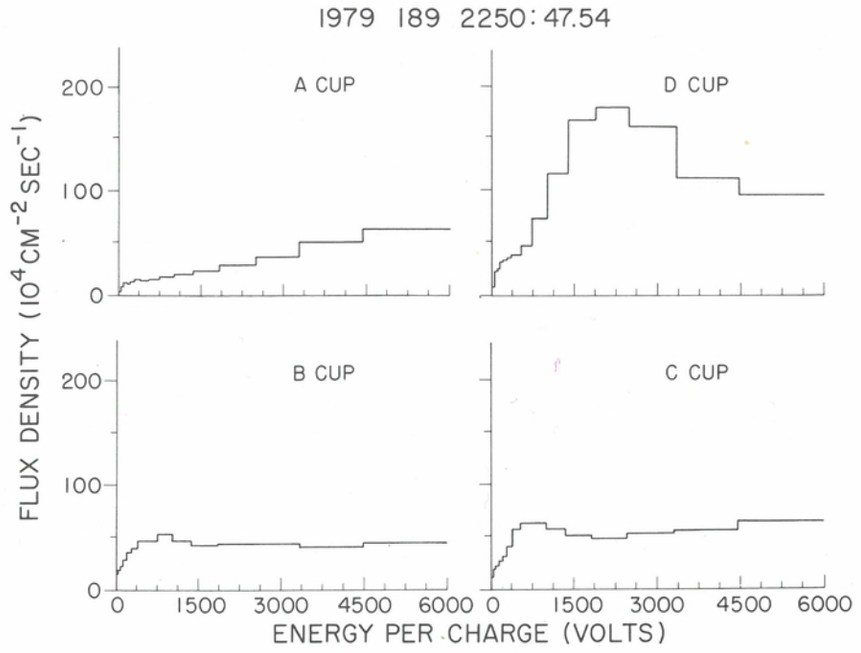

Fig. 3.21. The flux density of positive ion charge, in units of elementary charges per square centimeter per second, vs. energy per charge for a low resolution ion measurement from Voyager 2 inbound at 20.0 R_J.

Plasma velocities in the middle magnetosphere

Azimuthal flows. Bridge et al. [1979a,b] report that the low-energy plasma in the Jovian magnetosphere tends to move azimuthally about Jupiter. This statement is based on the observation that the relative magnitudes of the positive ion fluxes in the different sensors during the encounters correspond qualitatively to those expected for a cold corotating beam (Figs. 1 and 2 of McNutt, Belcher, and Bridge [1981]). An example of this behavior is shown in Figure 3.21. This is a low-resolution positive-ion spectrum obtained by Voyager 2 on July 8 at 2250 UT, when the spacecraft was 20 R_J from Jupiter. Rigidly corotating flow at this distance would appear at a speed of 240 km/s, with the aberrated flow velocity at angles of 95°, 69°, 64°, and 19° to the A, B, C, and D cup axes, respectively (0° is directly into the cup). Thus, one would expect to see corotating H^+ (O^{2+}) at an energy per charge of ~300 V (~2400 V) in the D cup, and at an energy per charge of ~75 V (~600 V) in the B and C cups. The positive-ion spectra in the B, C, and D cups in Figure 3.21 are consistent with the unresolved presence of H^+

plus heavy ions at roughly these energies. The low-energy shoulder in the D cup is probably H^+, with the higher-energy peak due to heavy ions. In the B and C cups, the H^+ shoulder disappears because of projection effects, and the heavy-ion peak moves to lower energies, and also lower fluxes, because of the cup response. For a cold beam, the A cup should show no response at this time, and thus the fluxes in the A cup must be due to the finite thermal spread of the beam. Qualitatively, it is clear from these spectra that at this distance the positive ions are reasonably supersonic and moving azimuthally to first order (radial and vertical motions may also occur, as discussed in the subsection entitled "Nonazimuthal flows," although in general these are second-order effects). This pattern holds through both the Voyager 1 and 2 encounters. Note that the equal flux levels in the B and C sensors in Figure 3.21 suggest that the vector velocity is more or less in the Jovian equatorial plane at this time, because the B and C sensors are symmetrically oriented south and north with respect to that plane (see Belcher and McNutt [1981], or McNutt, Belcher, and Bridge [1981]).

The D cup spectrum in Figure 3.21 is representative of ~70% or more of the low-resolution spectra obtained during the Voyager 1 encounter. The remaining 30% of the low-resolution spectra from Voyager 1 display a distinct separation between H^+ and the heavy ions, and they can be analyzed for temperatures, concentrations, and velocity components. In contrast, the only quantitative parameter that can be easily derived from unresolved ion spectra such as in Figure 3.21 is the elementary-charge concentration of positive ions in the energy range of the Plasma Science experiment. For example, the total flux density of positive-ion charge in the D cup spectrum of Figure 3.21 is 1.1×10^7 proton charges per square centimeter per second. This charge flux density is the product of the total elementary-charge concentration in this energy range, n_i, times the (common) ion-velocity component into the cup, V_n, provided that the latter is reasonably supersonic. Thus, if V_n is 200 km/s at the time of the spectrum in Figure 3.21, n_i must be 0.54 proton charges per cubic centimeter. The estimates of n_i in Figures 3.12 and 3.14 were obtained in this way, using a model for V_n obtained from the resolved ion spectra, as we now discuss.

For the resolved spectra in the D sensor on the inbound trajectory, the response function of that sensor to the plasma can reasonably be approximated by a constant. It is then directly possible to obtain from the measured currents estimates of plasma parameters describing the positive-ion distribution functions – for example, composition, concentration, temperature, and (in the case of a single sensor) that component of velocity along the sensor look direction. To obtain all three components of the plasma velocity, however, requires information from at least three sensors. As we have previously noted in the subsection entitled "Plasma velocities in the torus," in the cold inner torus, inside the orbit of Io, corotating flow is essentially parallel to the symmetry axis of the main cluster, and the response of each of the Faraday cups in the main cluster can be taken to be constant [Bridge et al., 1977]. In such a situation, the full vector velocity can be reconstructed with high accuracy from measurements in the A, B, and C sensors (see Table 3.2). In the dayside middle magnetosphere, however, all sensors except the D sensor are usually significantly oblique to the flow. Thus, vector velocites can only be obtained using an analysis based on the instrument response for ions that arrive at large angles to the detector normals in the main cluster. The numerical methods required for a multisensor analysis using the full response are well understood in principle, but they are complex to implement in practice. A systematic program to analyze quantitatively multisensor data in the middle magnetosphere and at the Io flux tube is in process (Barnett and Olbert, private communication, 1981). However, at present, quantitative estimates of velocities in the middle magnetosphere are limited to that component of velocity along the D sensor axis.

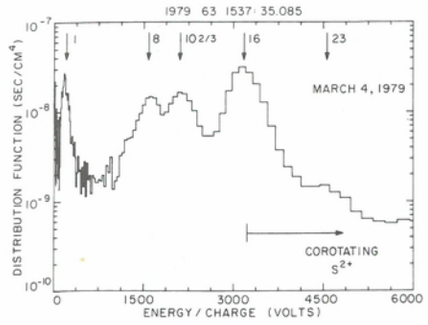

Fig. 3.22. A high resolution M-mode measurement from the D sensor of the positive-ion distribution function at 19.8 R_J. A least squares fit to the 8, 10.67, and 16 peaks yields a common velocity component of 195 km/s into the D sensor, and this velocity is used to draw the various arrows in the figure. The velocity component expected on the basis of rigid corotation is 238 km/s. The expected energy per charge of an S^{2+} ion moving at the rigid corotation speed is indicated.

The breakdown of corotation. In terms of single sensor analysis, the best determinations of the component of plasma flow into the D sensor in the middle magnetosphere are obtained from the cold ion spectra occurring in the plasma sheet crossings (see the subsection entitled "The plasma sheet"). Figure 3.22 is one of the best examples of a high-resolution ion spectrum with excellent species resolution. The common velocity component of the heavy ions in Figure 3.22 is 195 km/s, as compared to a component of 238 km/s expected for rigid corotation. The thermal width of the peak at an A/Z^* value of 16 in Figure 3.22 is only 11 km/s, so that this peak is 3.9 thermal widths below the expected corotation speed. One might argue that the lack of corotation displayed in this spectrum is due to various nonphysical effects – for example, spacecraft charging, or improper identification of ionic species. However, for this type of spectrum, the arguments for the observation of a true departure from rigid corotation are incontrovertible [McNutt et al., 1979; Belcher, Goertz, and Bridge, 1980; McNutt, Belcher, and Bridge, 1981]. The upper panel in Figure 3.23 shows values of V_n obtained from fits to such high-resolution spectra with resolved heavy ion peaks, as in Figure 3.22. There are not a large number of such spectra because the requirement of resolved heavy-ion peaks requires Mach numbers greater than about 6. However, these cold spectra occur systematically at the concentration maxima associated with the plasma sheet (see Figure 3.12). Thus, although they are few in number, they represent the speed of the plasma at the peak concentration in the middle magnetosphere. The departure from rigid corotation is systematic, growing with increasing Jovicentric distance.

The bottom panel of Figure 3.23 shows the values of V_n determined from fits to low-resolution ion spectra with a proton peak well separated from the heavy-ion peak. The value of V_n is determined mainly by the proton peak. There are many more of these spectra because the protons are more prominent in the wider energy windows of the low resolution mode and are well-resolved from the heavy ions down to Mach numbers as low as ~2. However, the uncertainties in the value of V_n so determined are much larger, because the energy resolution is coarser, and because the position of the light-ion peak is more strongly affected by possible spacecraft charging. Although these determinations agree with the high-resolution values when comparison is possible, it is the high-resolution values that argue convincingly for the breakdown of rigid corotation. Figure 3.24 shows values of V_n divided by the expected rigid component, using both high and low-resolution spectra, for both Voyager 1 and Voyager 2. There is some indication that the magnetospheric plasma was rotating more slowly through the dayside during the Voyager 2 passage.

Independent of and essentially simultaneous with these observations of a departure from strict corotation, Hill [1979, 1980] predicted on theoretical grounds the existence of such an effect owing to inertial loading (see the subsection entitled "Inertial loading"

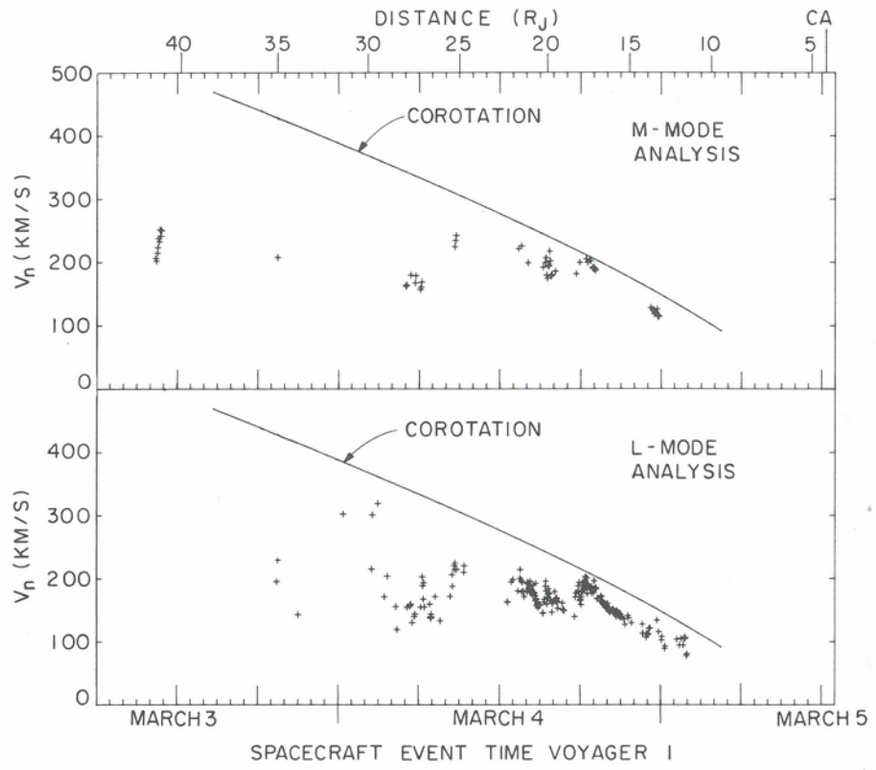

Fig. 3.23. Value of the component of velocity into the D sensor for Voyager 1 as determined from fits to low resolution (*L*-mode) and high resolution (*M*-mode) ion spectra. The component of velocity expected for rigid corotation is also shown.

and Chaps. 10 and 11). This theory is now the accepted explanation for the subcorotational velocities observed in the middle magnetosphere.

Nonazimuthal flows. In addition to the quantitative least-squares fit values of V_n from single-sensor analysis, more qualitative information about the full vector velocity can be obtained from multiple sensor data by taking advantage of the nearly symmetric orientation of the B and C cups with respect to the Jovian equatorial plane. Such an analysis suggests a general pattern of nonazimuthal flow that appears to be away from the equatorial current sheet on the dayside and toward it on the nightside [Belcher and McNutt, 1981; McNutt, Belcher, and Bridge, 1981]. Figure 3.25 illustrates this pattern qualitatively for Voyager 2; a similar phenomenon is seen in the Voyager 1 fluxes. This figure displays the difference of the total flux density of positive ions into the B cup and the total flux density into the C cup, divided by the sum of these two flux densities. Because the B cup opens southward and the C cup opens northward, this difference will be positive if there is flow to the north and negative if there is flow to the south. The horizontal axis is linear in spacecraft event time. Also indicated are radial distance from the planet and Universal Time at the top and local time at the bottom. The figure also shows the spacecraft position perpendicular to the magnetic equatorial plane.

Recall that passing through the magnetic equatorial plane essentially marks crossings of the Jovian current sheet, especially within 20 R_J of the planet. The main

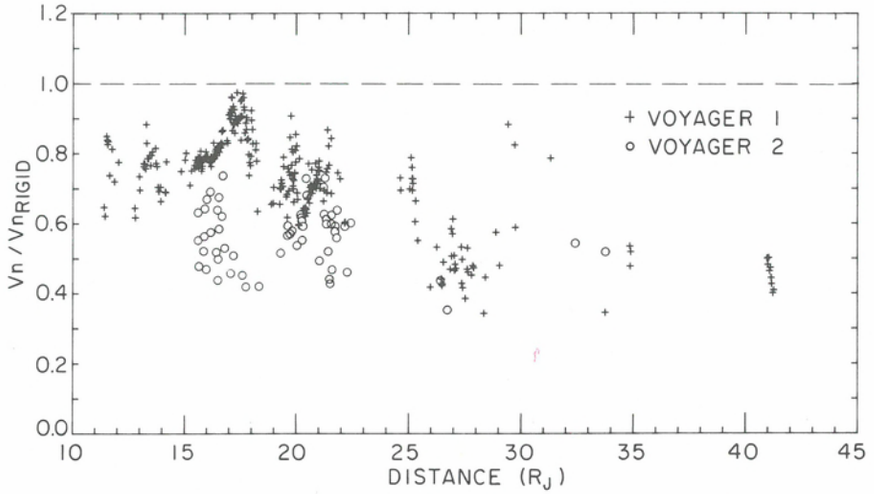

Fig. 3.24. The observed component of velocity into the D sensor divided by the component expected for rigid corotation for Voyagers 1 and 2.

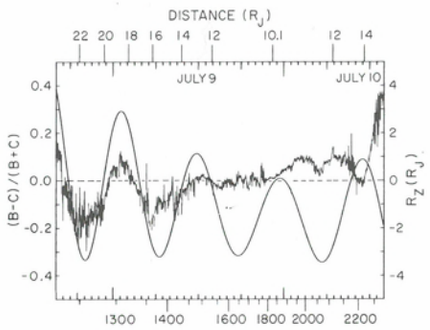

Fig. 3.25. A plot of the differences between the flux densities in the B and C cups divided by their sum for Voyager 2. Also shown is the vertical distance of the spacecraft from the magnetic dipole equatorial plane. Local time is indicated at the bottom and both distance from Jupiter and universal time at the top (the date is given at 1200 UT).

sensor is oriented such that there would be slightly more purely azimuthal flow into the C cup than the B cup on the inbound leg, and vice versa on the outbound leg. Even in the absence of any north/south flow, one would expect to see a negative signature in $(B - C)/(B + C)$ inbound and a positive signature outbound. In fact, the differences in Figure 3.25 oscillate about a negative average value inbound and a positive average value outbound, as expected. The oscillations about this mean imply that in the dayside magnetosphere near noon, there is a tendency for plasma flow to be northward when the spacecraft is north of the magnetic dipole plane, and southward when the spacecraft is south of that plane – that is, the flow is away from the current sheet. The amplitude of the difference decreases to zero with decreasing radius and increasing local time toward dusk. In the dusk to midnight sector, the difference again increases with increasing radius and increasing local time toward midnight. However, in this sector the plasma flow tends to be northward when the spacecraft is south of the magnetic equator, and vice versa – that is, the flow is now toward the current sheet.

Belcher and McNutt [1980] have suggested that these apparent flows away from and toward the equatorial region are caused by dynamic expansion and contraction of the plasma sheet resulting from the compression of the dayside magnetosphere by the solar wind. As flux tubes rotate into the dayside magnetosphere, they move closer to Jupiter and the plasma flows away from the equator due to the compression and to the

decreasing centrifugal force. On the nightside, the flux tubes move outward, and the plasma collapses back toward the equator due to the expansion and to the increasing centrifugal force. One obvious problem with this qualitative picture is the phase of the effect, because in the quasistatic approximation one would expect maximum compression and thus zero velocity near noon, not near dusk. On the other hand, the plasma sheet may not be in quasistatic equilibrium [see McNutt, Belcher, and Bridge, 1981], and thus there may be a phase lag due to dynamic overshoot and finite-propagation time effects. At present, there is no quantitative model, and such explanations remain conjectural.

3.5. The outer magnetosphere

In the dayside magnetosphere beyond about 50 R_J, the organized plasma sheet structure disappears. Even so, we still observe sporadic appearances of cold, dense concentrations of electrons and ions, correlated with decreases in magnetic field strength. Such regions appear similar in morphology to the spikey structure in the middle magnetosphere (see the subsection entitled "The plasma sheet"), except that they occur randomly, and not near expected crossings of the magnetic equator. Outside of the cool, dense regions, hot electrons with characteristic energies of a few keV appear to be the exclusive electron population. Positive-ion measurements in these hot regions are difficult to interpret both because of the low flux levels at these distances and because of the possibility of significant hot-electron feedthrough into the positive-ion measurements (see the discussion in McNutt, Belcher, and Bridge [1981]). Overall, the dayside outer magnetosphere appears to be a disordered and turbulent region in its plasma characteristics.

In contrast, the nightside magnetosphere is well organized by the plasma sheet structure out to great distances. On Voyager 1 outbound, regular enhancements in electron concentration were measured by the Plasma Science experiment, occurring twice per planetary rotation period out to 85 R_J, and once per rotation period out to 120 R_J. The location and time of these crossings of the predawn plasma sheet have been studied extensively [e.g., Goertz, 1981], and will not be discussed here. As we have noted above in the subsection entitled "The Voyager Plasma Science experiment," positive-ion observations outbound on the Voyagers were of poor quality for the most part because of the unfavorable viewing geometry.

3.6. Discussion

Sources of plasma

Given the observed properties of the low energy plasma at Jupiter, a number of authors have considered the nature of the sources, transport mechanisms, and energy and angular momentum balance in that plasma. We briefly review some of these considerations in light of the above phenomenology. The detection of an SO_2 atmosphere by Pearl et al. [1979] and SO_2 frost on the surface of Io [Fanale et al., 1979; Smythe, Nelson, and Nash, 1979] make SO_2 an obvious source material for the magnetosphere. However, Bagenal and Sullivan [1981] observe more sulfur in the torus than expected from the full dissociation and ionization of SO_2. Unfortunately, the characteristics of the dissociation and ionization processes for SO_2 are not well known. Shemansky [1980b] suggests that they probably involve O_2 and SO molecules and their ions. The existence of intermediate dissociation products of SO_2 as well as the fact that oxygen is less readily ionized than sulfur may explain why more sulfur was observed in the torus

than expected. In addition, there must be some mechanism (such as sputtering) for the removal from Io of material that is not a major constitutent of the atmosphere (e.g., consider neutral sodium, which has been observed in the magnetosphere for many years). Because there is probably a significant amount of elemental sulfur on the surface of Io [Masursky et al., 1979], additional sulfur may be supplied to the torus by such a process.

Although the ultimate source for the torus plasma is Io, it is not clear where the ionization takes place. The plasma could come either from the ionization of a diffuse cloud of neutral gases spread over a large portion of Io's orbit, or from the immediate vicinity of Io itself in the complex interaction of the magnetospheric plasma and the satellite. For a diffuse source, freshly ionized particles gain a cyclotron speed equal to the magnitude of the difference between the original velocity of the neutral atom and the local corotation velocity. At 6 R_J, sulfur and oxygen would gain cyclotron energies of 545 and 270 eV, respectively. Because the observed temperature of the bulk of the ions in the torus is ~ 40 eV, a diffuse source requires an efficient mechanism for the removal of most of this initial cyclotron energy. In contrast, the localized source can produce ions that initially pick up much smaller cyclotron energies, owing to the reduction of the local corotational electric field in the immediate vicinity of Io [Goertz, 1980a]. However, the Voyager ultraviolet measurements indicated that there was no enhancement of emission in the vicinity of Io [Shemansky, 1980b] as would be expected if the source were localized there. In addition, the existence of an extensive cloud of neutral sodium and the recent observation of neutral oxygen in the vicinity of Io's orbit [Brown, 1981a] suggest that the sulfur and oxygen ions may come from extended clouds of neutral atoms. The conclusion of Brown and Ip [1981], and Bagenal and Sullivan [1981], that there may be significant fraction of S^+ ions with energies far higher than the average energy of the torus, also supports the notion of diffuse pickup of new ions at large cyclotron energies followed by rapid dissipation of energy to the observed ion temperatures (see also Chap. 6).

Diffusive transport

In any case, new ions enter the torus from a source region localized either to the vicinity of Io or its orbit. They eventually diffuse away from the source under the controlling infuence of centrifugal force, which aids outward but inhibits inward transport [Richardson et al., 1980; Richardson and Siscoe, 1981; Siscoe and Summers, 1981]. To investigate the nature of this diffusive transport of plasma, Bagenal and Sullivan [1981] computed the total number of ions in a unit L-shell times L^2 (i.e., NL^2). This quantity is plotted in Figure 3.26 as a function of distance from Jupiter. The total tube content had a maximum at ~ 5.7 R_J and decreased monotonically radially inward and outward from the peak. Although the concentration along the spacecraft trajectory exhibited three local maxima at different radial distances, the flux tube content has only a single peak, which supports the model of diffusion of plasma from a single source near Io.

Siscoe et al. [1981] have made the most detailed effort to date to interpret these observations of flux tube content in terms of the mass transport theory appropriate for flux tube interchange diffusion. As illustrated in Figure 3.26 from Siscoe et al. [1981], the inner magnetosphere can be divided into four different diffusion regions according to the differing slopes of NL^2 vs. L in these regions. Large slopes indicate zones of weak diffusion and small slopes zones of strong diffusion. The innermost region contains the cool inner torus, and is referred to as the precipice to describe the sharp decrease in total mass and temperature observed there. The warm Io torus is referred to as the ledge, and is separated from the inner edge of the plasma disc or sheet by the ramp. The

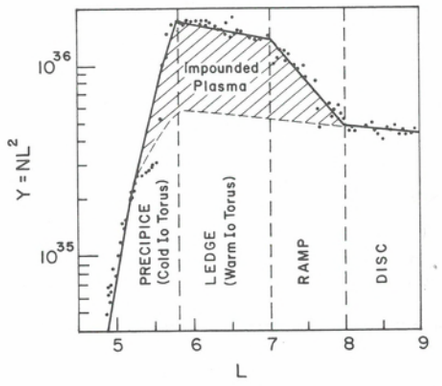

Fig. 3.26. Radial profile of the magnetic flux shell density $Y = NL^2$, where N is the number of ions in a flux shell per unit L.

sharp break in the slope of NL^2 at $L = 5.8$ is the likely location of the inner edge of the source region, and therefore marks the separation between the domains of inwardly and outwardly diffusing ions. The steep slope in the precipice demonstrates that inward diffusion "uphill" against the centrifugal force is comparatively feeble. The relatively small amount of inwardly diffusing plasma is transported slowly, and so has time to cool by radiation. As the plasma cools, it collapses toward the centrifugal equator, and the resulting increase in the local density enhances the emission so that the plasma cools further. This runaway process leads to the sharp transition in temperature and ionization states between the regions of inward and outward diffusion.

In contrast, 90% of the injected plasma rapidly diffuses outward to replenish the ledge, and does not have time to cool by radiation. The shallow gradients distinguishing the plasma ledge and the plasma disc illustrate the situation expected when centrifugally driven interchange instability is restrained only by ohmic dissipation in Jupiter's ionosphere [Siscoe and Summers, 1981]. The much steeper decline delineating the plasma ramp signifies a substantially diminished level of diffusive activity. The origin of this feature is attributed by Siscoe et al. [1981] to pressure gradient inhibition of the interchange motion enforced by a prominent precipitation edge to the ring current that coincides with the ramp [Krimigis et al., 1979a]. The base of the hatched area in Figure 3.26 depicts the shape the Io plasma formation would have if there were no ring current. The hatched area itself indicates the amount of Io plasma supported against the outward centrifugal force by the inwardly directed pressure of the inner surface of the ring current. The quantity of matter impounded in this way is very nearly equal to the total bulk of the plasma ledge alone. Bagenal and Sullivan [1981] estimate that the total mass of the ledge (i.e., the warm torus) is 1×10^{36} amu.

Inertial loading

As diffusion continues outward through the ramp and into the extended plasma disc, the diffusing plasma must be accelerated to higher azimuthal velocities with increasing radial distance in order to maintain corotation with the planet. At larger distances, the energy and angular momentum requirements for this continued acceleration becomes an increasing strain on the frictional coupling between the Jovian ionosphere and the neutral atmosphere, and eventually at large enough distances the magnitude of this frictional coupling is no longer sufficient to maintain rigid corotation [Hill, 1979]. Hill [1980] has calculated a mass-loading rate of $\sim 10^{30}$ amu/s in order to account for the marked deviation from corotation observed by the Plasma Science experiment beyond

20 R_J [McNutt et al., 1979]. It is worth emphasizing that the Plasma Science instrument cannot determine velocity components beyond $\sim$ 40 R_J because of the lack of well-resolved, cold ionic spectra in the outer magnetosphere. However, measurements by the Low-Energy Charged Particle experiment also provide estimates of the plasma velocity under certain assumptions, and on Voyager 1 inbound the two different velocity measurements agree when they can be compared [Carbary et al., 1981]. The estimates of velocities from the Low-Energy Charged Particle experiment in the outer magnetosphere show that ion velocities there again become reasonably close to those expected of full corotation (see Chapter 4). Such behavior of velocity with distance cannot be explained by the inertial loading model of Hill, and is not understood theoretically at the present time.

The middle and outer magnetosphere

In contrast to the large effort that has been directed at understanding the physics of the Io torus, there have been relatively few post-Voyager attempts to understand the physical mechanisms that control the thermal properties and dynamics of the plasma in the middle and outer magnetosphere. Most obviously, it is unclear what source of energy keeps the bulk of the low-energy ions from adiabatically cooling as they diffuse outward. The heating mechanism may be related to the compression of the dayside magnetosphere due to the solar wind interaction [i.e., Goertz, 1978; Belcher and McNutt, 1980]. This same mechanism may be responsible for the energic ion component discussed in Chapter 4. Just as puzzling is the thermal stratification in the sheet. It may be that the hotter, higher latitude ions have a different temporal history as compared to the cool ions at the concentration maxima, as has been suggested for the suprathermal electron population adjacent to the sheet. Scudder, Sittler, and Bridge [1981] suggest that the suprathermal electrons (i.e., the 2–3 keV "bath" of hot electrons at higher latitudes), are a natural consequence of the peculiar situation of closed field lines being simultaneously above two different exobases, one at the ionospheric foot of the flux tube, with the other at the centrifugal equator. In this situation, the small population of electrons that can escape the respective exobases will find a natural place in the midlatitude regions. Thus, there may be no need for an energization process for these suprathermal electrons.

In addition to the thermal properties, the existence of nonazimuthal flow velocities in the middle magnetosphere (e.g., flows away from and toward the plasma sheet) is of interest since it bears on the overall dynamics of the plasma sheet. Quantitative models of the plasma sheet dynamics in light of the Voyager observations require additional observational and theoretical input. Future progress in our understanding of this region depends on more thorough analysis of the data from the various experiments, as well as on detailed cooperative studies. The middle and outer magnetosphere is the region of greatest promise in terms of potentially dramatic increases in our understanding of the important physical processes in the Jovian magnetosphere.

ACKNOWLEDGMENT

The success of the Voyager Plasma Science experiment is due to the leadership of Professor H. S. Bridge, Principal Investigator. I am grateful to F. Bagenal, H. S. Bridge, R. McNutt, Jr., J. Scudder, and E. Sittler, Jr. for a careful reading of the manuscript and many constructive suggestions. This work was supported under JPL contract 953733 and NASA contract NGL22-009-015.